



PERGAMON

Deep-Sea Research II 49 (2002) 4715–4742

DEEP-SEA RESEARCH  
PART II

www.elsevier.com/locate/dsr2

## On the export of Antarctic Bottom Water from the Weddell Sea

Alberto C. Naveira Garabato<sup>a,\*</sup>, Elaine L. McDonagh<sup>a,1</sup>, David P. Stevens<sup>b</sup>,  
Karen J. Heywood<sup>a</sup>, Richard J. Sanders<sup>a,2</sup>

<sup>a</sup>*School of Environmental Sciences, University of East Anglia, Norwich NR4 7TJ, UK*

<sup>b</sup>*School of Mathematics, University of East Anglia, Norwich NR4 7TJ, UK*

Accepted 16 March 2002

### Abstract

A survey of the current field over the South Scotia Ridge, obtained with a lowered Acoustic Doppler Current Profiler (LADCP), is presented. There is a pattern of northward (southward) flow on the western (eastern) side of each of four deep passages in the ridge, which is supported by tracer measurements. The net full-depth LADCP-referenced geostrophic transport over the ridge is  $22 \pm 7$  Sv ( $1 \text{ Sv} = 10^6 \text{ m}^3 \text{ s}^{-1}$ ) northward, with the jets on either side of the passages transporting 5–10 Sv in alternating directions. The corresponding Weddell Sea Deep Water (WSDW) transport over the ridge is  $6.7 \pm 1.7$  Sv. This is a factor of 4 larger than the only previous estimate in the literature, and suggests that a significant proportion of the Antarctic Bottom Water (AABW) invading the world ocean abyss escapes the Weddell Sea via the Scotia Sea.

The net full-depth and WSDW transports over the ridge are modified to  $7 \pm 6$  and  $4.7 \pm 0.7$  Sv, respectively, by a box inverse model of the western Weddell Gyre. The model incorporates the WOCE A23 crossing of the central part of the gyre and a set of five constraints synthesizing our previous oceanographic knowledge of the region. It diagnoses that  $9.7 \pm 3.7$  Sv of AABW are formed in the Weddell Sea, and that comparable amounts are exported over the South Scotia Ridge ( $\sim 48\%$ ) and further east ( $\sim 52\%$ ) assuming that no AABW enters the Weddell Gyre from the Indian Ocean. The WSDW fraction with neutral density  $\gamma^\theta > 28.31 \text{ kg m}^{-3}$  transported over the ridge upwells in the Scotia Sea at a rate of  $6 \times 10^{-6} \text{ m s}^{-1}$ , an order of magnitude larger than many basin-scale estimates of deep upwelling in the literature. In contrast, the Weddell Sea Bottom Water exported to the eastern Weddell Gyre entrains upward at a rate of  $8 \times 10^{-7} \text{ m s}^{-1}$ , more typical of other open-ocean regions. When their different ventilation histories are considered, the comparable transports and disparate upwelling rates of the AABW exported over the South Scotia Ridge and farther east may be crucial to our understanding of teleconnections between the Weddell Sea and the global ocean.

© 2002 Elsevier Science Ltd. All rights reserved.

\*Corresponding author. Fax: +44-1603-507719.

E-mail address: a.naveira-garabato@uea.ac.uk (A.C. Naveira Garabato).

<sup>1</sup>Present address: James Rennell Division, Southampton Oceanography Centre, Southampton SO14 3ZH, UK.

<sup>2</sup>Present address: George Deacon Division, Southampton Oceanography Centre, Southampton SO14 3ZH, UK.

### 1. Introduction

Antarctic Bottom Water (AABW) is the densest of the water masses implicated in the thermohaline circulation of the world ocean (Orsi et al., 1999). Its formation takes place at a few locations around

the Antarctic continental margins where Circumpolar Deep Water (CDW), entrained southward from the Antarctic Circumpolar Current (ACC), is brought into contact with very cold and dense shelf waters. The ensuing interaction between the two water types produces convecting plumes that descend along the continental slope and replenish the AABW layer offshore. Examination of the hydrography near Antarctica has led to the identification of a number of sites where AABW can potentially be produced, namely between the Enderby Land coast and the western Ross Sea in the Indian–Pacific sector, and in the southwestern and western Weddell Sea in the Atlantic sector (Whitworth et al., 1998). Quantitative studies to date have suggested a dominance of the Atlantic sources. From water-mass analyses, Carmack (1977) estimated that about 70% of the AABW in the Southern Ocean is affected by water-mass formation in the Weddell Sea, whereas Orsi et al. (1999) diagnosed from the oceanic chlorofluorocarbon budget that 60% of the circumpolar production of AABW occurs in the Atlantic sector. The numerical model results of Hellmer and Beckmann (2001) suggest a slightly lower relative contribution of Atlantic sources (just over 50%).

Circulation in the Weddell Sea (Fig. 1) is dominated by the cyclonic Weddell Gyre, which extends from the Antarctic Peninsula to 30°E (Orsi et al., 1993). Near this longitude, a broad discontinuity in the Southwest Indian Ridge allows the injection of CDW into the eastern limb of the gyre. This CDW is then transported westward along the southern branch of the gyre, gradually cooling and freshening as it entrains ambient waters, and is commonly referred to as Warm Deep Water (WDW) due to its ambient characteristics. West of 30°W, WDW interacts with the dense shelf waters off the Filchner-Ronne Ice Shelf (Whitworth et al., 1998) and AABW formation occurs. Although the environs of the Filchner-Ronne Ice Shelf have been traditionally regarded as the principal source region of AABW in the Weddell Sea, significant AABW production has been reported off the eastern Antarctic Peninsula, particularly near the Larsen Ice Shelf (Fahrbach et al., 1995; Weppernig et al., 1996; Gordon, 1998).

The newly formed AABW is conveyed northward in the western limb of the Weddell Gyre and may escape the Weddell Sea along two distinct sets of pathways. Early works (e.g., Gordon, 1966) considered bottom potential temperature distributions as evidence of a spreading route of AABW along the South Sandwich Trench, and other studies (Orsi et al., 1993, 1999) noted that AABW can leave the Weddell Sea along the South Sandwich Abyssal Plain and the region of the gyre east of the mid-Atlantic Ridge. More recently, the possibility of AABW export over the South Scotia Ridge (which separates the Weddell Sea from the Scotia Sea to the north) being an important outflow from the Weddell Sea has been recognised (Locarnini et al., 1993). However, owing to the sparsity of sampling in the region, this export remains poorly quantified. Locarnini et al. (1993) estimated a northward geostrophic transport of 1.5 Sv ( $1 \text{ Sv} = 10^6 \text{ m}^3 \text{ s}^{-1}$ ) of AABW (relative to 1500 m) through the Orkney Passage, the deepest gap in the South Scotia Ridge. Direct current measurements north of the ridge (Gordon et al., 2001) and the detection of AABW overflowing the ridge at other locations (Locarnini et al., 1993; Naveira Garabato et al., 2002) suggest that this figure might be an unrepresentative measure of the net AABW export over the ridge.

The dichotomy in the escape pathways of AABW out of the Weddell Sea relates closely to a distinction between two regional forms of AABW made by Carmack and Foster (1975) based on water-mass properties and distributions: the lighter Weddell Sea Deep Water (WSDW) can overflow the South Scotia Ridge, whereas the denser Weddell Sea Bottom Water (WSBW) cannot (e.g., Naveira Garabato et al., 2002). WSBW is colder and fresher than WSDW, contains higher concentrations of atmospheric gases (Mensch et al., 1997), and is separated from the latter by a stability maximum (Reid et al., 1977). For these reasons, WSBW has been traditionally regarded as the more recently ventilated of the two, and WSDW as a linear mixing product of WSBW and the overlying WDW. Direct formation of WSDW from mixing of shelf waters and WDW, of which there is evidence (e.g., Weppernig et al., 1996), often has been presumed

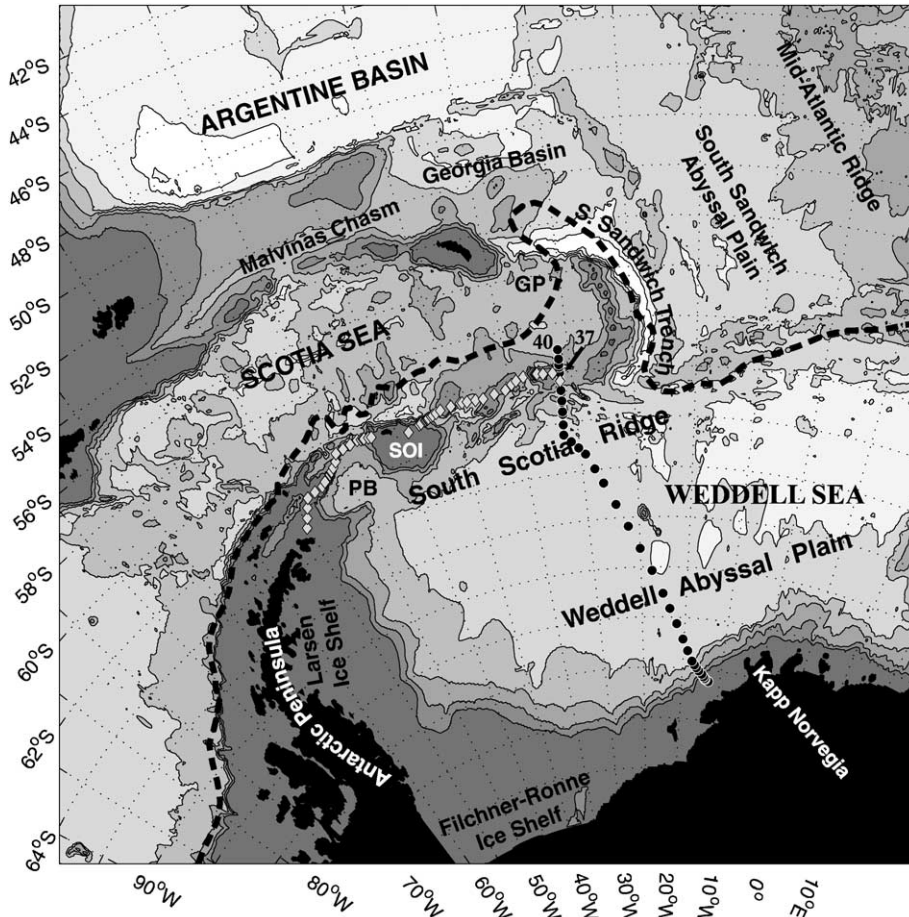


Fig. 1. Bathymetry (ETOP05) of the Weddell Sea and neighbouring basins (the contour interval is 1000 m). The locations of the WOCE A23 and ALBATROSS stations used in this study are marked by black dots and light-shaded diamonds, respectively. The Southern Boundary of the ACC is shown by the thick dashed line. Geographical features mentioned in the text are labelled (GP=Georgia Passage, SOI=South Orkney Islands, PB=Powell Basin). The positions of WOCE A23 stations 37 and 40 are indicated. Note that the eastern rim of the Weddell Gyre lies outside the map.

unimportant, and AABW production in the Weddell Sea quantified solely in terms of WSBW [see Gordon (1998) and references therein].

In this paper, we adopt a different approach to determining how much AABW is formed in the Weddell Sea, shifting the focus from the regions where AABW is produced to those where it is exported to the mid-latitude ocean basins. AABW from the Weddell Sea invades a number of major basins in the South Atlantic and Southwest Indian Oceans, overriding all other water masses as it

penetrates northward. Quantifying the net AABW export from the Weddell Sea and uncovering the partitioning of this export amongst different pathways is, therefore, central to understanding the global thermohaline circulation. This is illustrated by Rintoul (1991) in his study of interbasin exchange in the South Atlantic, where the prescribed rate of Weddell Sea AABW production has a marked impact on the meridional heat flux carried by the ocean at lower latitudes.

We commence by presenting a comprehensive survey of the circulation and transport of WSDW over the South Scotia Ridge. We show that flow over the ridge indeed represents a significant component of the AABW export from the Weddell Sea, and that the associated transport is substantially larger than that estimated by Locarnini et al. (1993) for the Orkney Passage. To quantify the net AABW export, we combine the South Scotia Ridge data set with an oceanographic section crossing the central Weddell Gyre (thus enclosing all the sites of AABW formation in the Weddell Sea) in a box inverse model of the region (Fig. 1). Our approach resembles that of Fahrback et al. (1994), who used direct hydrographic and current measurements to quantify water-mass conversions south of a transect between the tip of the Antarctic Peninsula and Kapp Norvegia, but has two added strengths. Firstly, employing a box inverse model enables us to force the results to be consistent with a set of dynamical constraints and ancillary information from a number of sources, as well as to explore the sensitivity to different parameters. Secondly, the availability of oceanographic data above the sill of the South Scotia Ridge provides the model with the ability to distinguish between AABW outflowing via the Scotia Sea and that exported further east.

## 2. Data set and hydrographic background

### 2.1. The data set

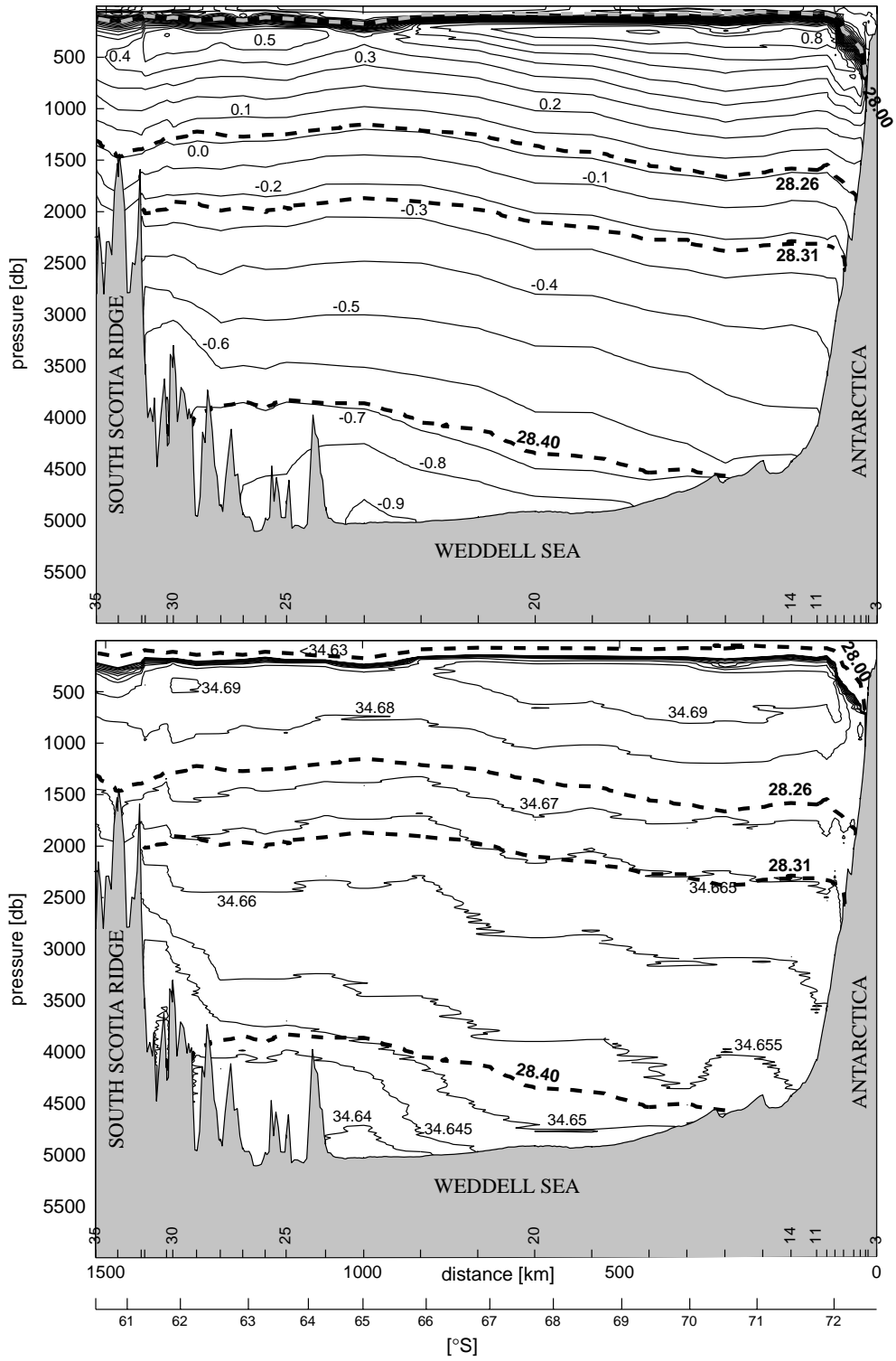
The data were collected during two cruises of the RRS *James Clark Ross*. Between 30 March and 8 April 1995, a segment of the World Ocean Circulation Experiment (WOCE) section A23 crossed the Weddell Sea quasi-meridionally between 16°W and 31°W. The second transect was performed between 31 March and 8 April 1999 along the South Scotia Ridge as part of the

ALBATROSS expedition. Locations of hydrographic stations are shown in Fig. 1.

During WOCE A23 a Neil Brown Mark IIIb CTD was used. The data collection and analysis methods are described in the cruise report (Heywood and King, 1996). The accuracies are 0.001°C in temperature and 0.002 in salinity. Horizontal current velocities were obtained at the southern end of the section using a vessel-mounted Acoustic Doppler Current Profiler (VMADCP). These are described by Heywood et al. (1998), who estimated the accuracy of VMADCP velocities to be 1 cm s<sup>-1</sup> there.

At ALBATROSS stations a Neil Brown Mark IIIc CTD was deployed with a 24-bottle rosette multisampler and a RDI 150 Hz BroadBand lowered ADCP (LADCP). The accuracies are 0.001°C in temperature and better than 0.002 in salinity, with precisions of 0.14% in oxygen and 1.37% in phosphate (Heywood and Stevens, 2000). The LADCP has an instrumental accuracy of 1 cm s<sup>-1</sup>, but a greater uncertainty is introduced by the determination of the barotropic component of the flow. This component was derived either from the displacement of the vessel as recorded by differential GPS (water-tracking) or, when the instrument was within ~200 m of the bottom, from the motion of the LADCP relative to the ocean floor (bottom-tracking) (Fischer and Visbeck, 1993). LADCP velocities were averaged in 20 m bins, and the tidal component subtracted using version 3.1 of the Oregon State University global tidal model (Egbert et al., 1994). The tidal contribution had a typical magnitude of 2 cm s<sup>-1</sup> east of the South Orkney Islands (Fig. 1), increasing to 5 cm s<sup>-1</sup> in the shallower region west of the islands and even higher values near the Antarctic continental shelf. We estimated the characteristic accuracy of the barotropic component of the LADCP flow as 3 cm s<sup>-1</sup> by calculating the root-mean-square (rms) deviation between water-tracking and bottom-tracking velocities over their common depth range.

Fig. 2. Vertical distribution of potential temperature (above) and salinity (below) along the WOCE A23 crossing of the Weddell Sea. Dashed lines represent the isopycnic water mass boundaries defined in Section 2.2 ( $\gamma^{\theta} = 28.00, 28.26$  and  $28.40 \text{ kg m}^{-3}$  mark the AASW/WDW, WDW/WSDW and WSDW/WSBW interfaces, with  $\gamma^{\theta} = 28.31 \text{ kg m}^{-3}$  as the boundary between the Upper and Lower classes of WSDW). Station positions are marked in the lower axes.



## 2.2. Hydrographic background

We use the neutral density variable ( $\gamma^n$ ) developed by Jackett and McDougall (1997) to define boundaries between the four major water masses encountered in the two transects. Neutral density values of 28.00, 28.26 and 28.40 kg m<sup>-3</sup> are selected as the Antarctic Surface Water (AASW)/WDW, WDW/WSDW and WSDW/WSBW interfaces, respectively. The first of these indicates the boundary between the Upper and Lower sublayers of CDW in Drake Passage (Naveira Garabato et al., 2002). As the Southern Boundary of the ACC coincides with the poleward edge of the Upper sublayer of CDW (Orsi et al., 1995), this boundary is a reasonable approximation to the density of the lightest CDW injected into the eastern Weddell Gyre from the ACC and later transformed to WDW. The second value ( $\gamma^n = 28.26$  kg m<sup>-3</sup>) separates WSDW from ACC waters in the Scotia Sea (Naveira Garabato et al., 2002). It differs slightly from Orsi et al.'s (1999) upper bound of AABW ( $\gamma^n = 28.27$  kg m<sup>-3</sup>). Their criterion in selecting that isopycnal was to exclude the densest water present at the still of Drake Passage, which conflicts with observations of a small volume of WSDW there (Naveira Garabato et al., 2002). Finally,  $\gamma^n = 28.40$  kg m<sup>-3</sup> coincides with the  $\theta = -0.7^\circ\text{C}$  isotherm [the WSDW/WSBW boundary originally defined by Carmack and Foster (1975)] in the northern Weddell Sea. We have chosen an additional neutral density surface ( $\gamma^n = 28.31$  kg m<sup>-3</sup>) to subdivide the WSDW into an Upper and a Lower class. The latter is too dense to overflow the Georgia Passage (Fig. 1), which, apart from the passages in the South Scotia Ridge, is the only WSDW pathway out of the basin (Arhan et al., 1999; Naveira Garabato et al., 2002).

The potential temperature, salinity, and water-mass boundaries along the WOCE A23 crossing of the Weddell Gyre are shown in Fig. 2. The reader is referred to Heywood and King (2001) for a detailed discussion of the hydrography. A large-scale doming of property contours, centred just north of 65°S and associated with the cyclonic gyre circulation, is apparent. In the southern end of the section, an abrupt plunging of isolines towards Antarctica characterises the westward-flowing jet

of the Antarctic Slope Front (Heywood et al., 1998). Deep property contours are also depressed over the South Scotia Ridge, near which a weakening of the mid-depth potential temperature and salinity maxima is observed. These are signatures of the Weddell-Scotia Confluence, a quasi-zonal band of eastward flow and low stratification containing a high proportion of shelf water mixtures from the northwestern Weddell Sea (Whitworth et al., 1994).

AASW is observed occupying an approximately 100-m deep surface layer, except south of the Antarctic Slope Front where the layer thickens to 500 m. The WDW below is typified by mid-depth potential temperature and salinity maxima and extends down to approximately 1300 m. South of the gyre axis, the potential temperature and salinity maxima are most pronounced ( $\theta > 0.8^\circ\text{C}$ ,  $S > 34.71$ ) due to the relative proximity of the CDW inflow from the ACC, whereas they are weaker ( $\theta < 0.6^\circ\text{C}$ ,  $S < 34.70$ ) north of the axis. One cause for this weakening is interaction with the shelf waters of the western Weddell Sea, conducive to AABW formation and a northward reduction in the thickness of the WDW layer.

Below WDW, the WSDW layer shoals towards the north in response to the decreasing WDW volume. The WSDW layer thickness remains largely unaltered as the gyre is crossed, though a marked thickening of the sublayer with  $\theta < -0.4^\circ\text{C}$  and  $S < 34.66$  is detected near 61.5°S. This suggests the presence of a deep current core supported by the South Scotia Ridge, in line with direct current measurements at locations over the southern flank of the ridge further west (Barber and Crane, 1995; Gordon et al., 2001). WSBW is observed between 71°S, where the basin is deeper than 4500 m, and 62°S, where its upper boundary intersects the South Scotia Ridge at about 4000 m. Its thickness increases northward as the WDW layer thickness decreases. The coldest ( $\theta < -0.9^\circ\text{C}$ ) and freshest ( $S < 34.64$ ) WSBW in the transect lies at the axis of the gyre.

Many of the hydrographic features observed across the Weddell Sea are re-encountered above the sill of the South Scotia Ridge (Fig. 3), which is embedded in the Weddell-Scotia Confluence (Orsi et al., 1993). A detailed description of the

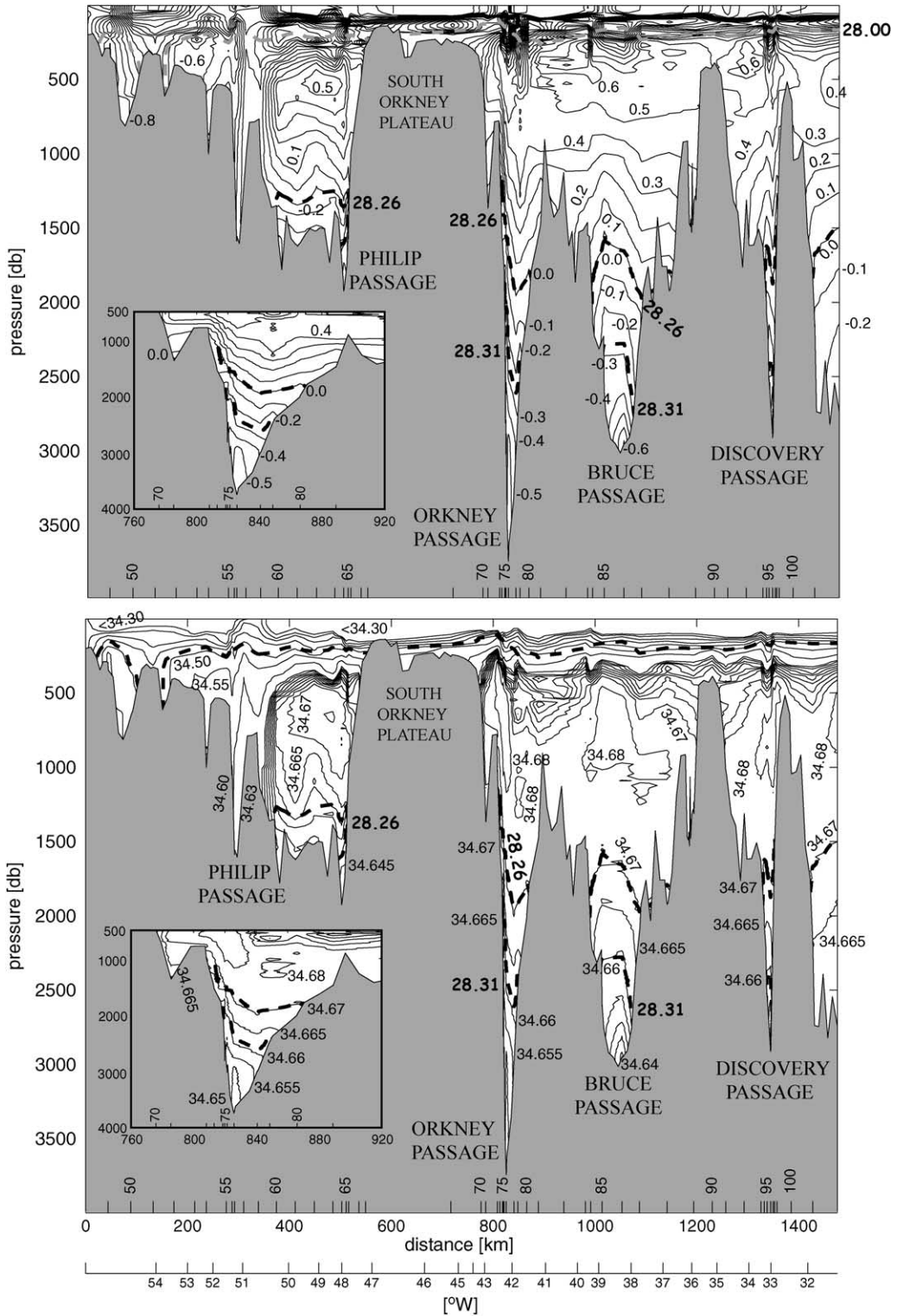


Fig. 3. As for Fig. 2, but for the ALBATROSS South Scotia Ridge transect. The deep Orkney Passage is expanded in the insets.

hydrography along this section can be found in Naveira Garabato et al. (2002). The Antarctic Slope Front is crossed just west of 50°W, as evidenced by the marked lateral property gradients. West of the front, the density ranges of AASW and WDW are occupied by relatively cold and fresh mixtures of these water masses with shelf waters. East of the front, the large variability in the potential temperature and salinity of WDW reflects various degrees of interaction with CDW from the ACC and shelf water mixtures in the Weddell-Scotia Confluence. WSDW is observed overflowing the ridge at four deep passages. In the three eastern passages (Orkney, Bruce and Discovery Passages) the interface between WDW and WSDW is often deeper than 1500 m and there are pronounced across-passage changes in the depth of isopycnals (of as much as 700 m). In the Philip Passage, however, this water-mass boundary is shallower and of broadly constant depth (1300 m). Note that the depth of the Orkney Passage (3800 m) is approximately equal to that at which the interface between WSDW and WSBW intersects the South Scotia Ridge (Fig. 2), i.e. no water in the WSBW density class overflows the ridge.

### 3. The WSDW overflow at the South Scotia ridge

The cross-track horizontal velocity measured by the LADCP (Fig. 4) shows that the flow over the South Scotia Ridge is largely barotropic. There is a clear pattern of northward (southward) flow on the western (eastern) side of each deep passage, consonant with model predictions (Pedlosky, 1994). The largest velocities (approaching 50 cm s<sup>-1</sup>) along the transect are observed over the western flank of the Orkney Passage near 2500 m. At the Antarctic Slope Front, near 50.5°W, deep currents exceed 20 cm s<sup>-1</sup>, and flows of about 10 cm s<sup>-1</sup> are measured at mid-depths

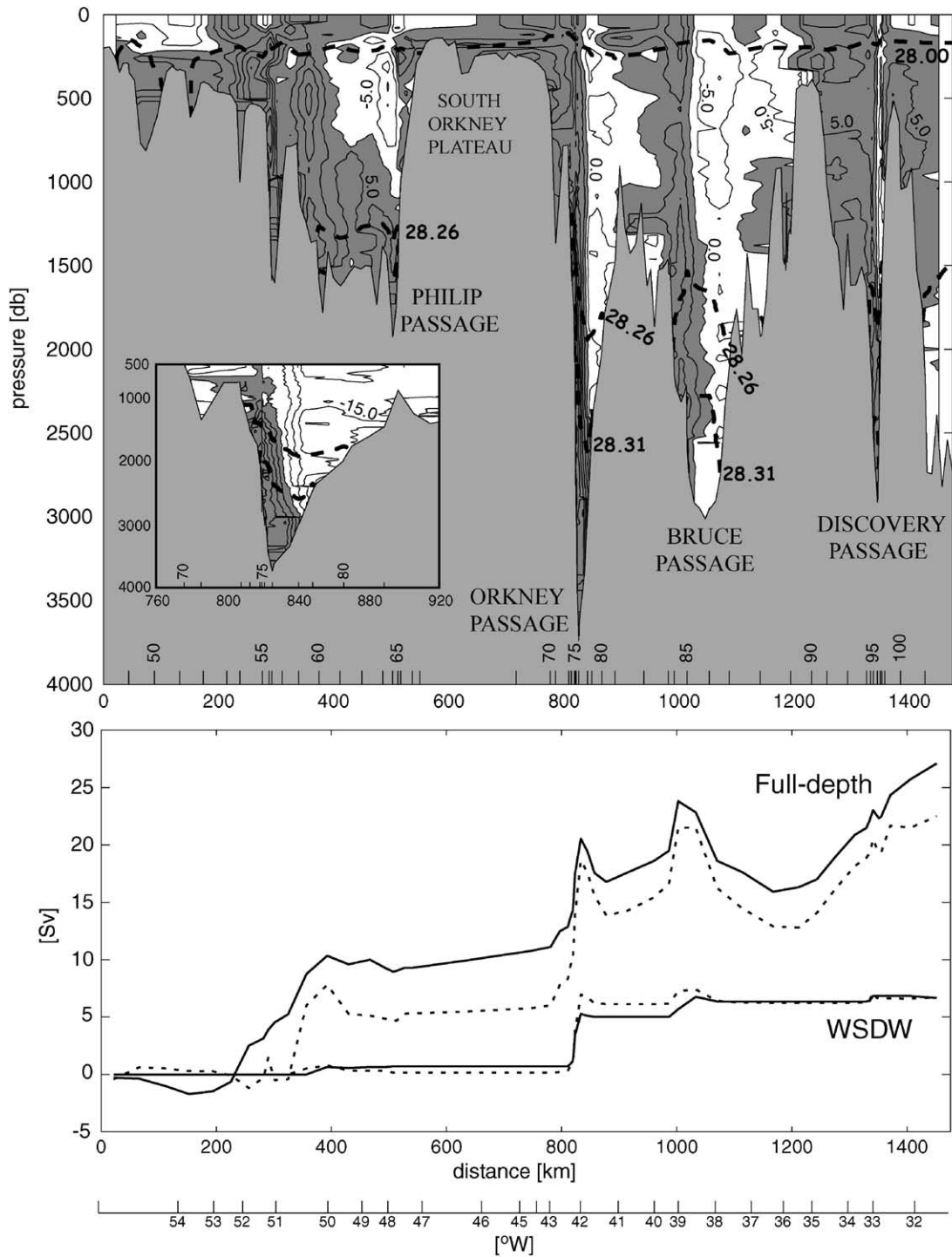
over the western flank of the Philip and Bruce Passages. On average, northward flows are more vigorous and extensive than southward flows. This feature is particularly pronounced in the WSDW density range (Fig. 5), implying a net northward export of WSDW over the ridge. Also note a tendency for the flow to be aligned perpendicular to the sill of the three eastern passages.

The remarkable coherence in the spatial patterns of measured flow suggests that our velocity record is largely free of contamination from high-frequency motions. Independent support for the dominant circulation pattern seen in the LADCP measurements was extracted from the distribution of the quasi-conservative water-mass tracer PO<sub>4</sub><sup>\*</sup> (Broecker et al., 1998), defined as

$$PO_4^* = PO_4 + O_2/175 - 1.95 \mu\text{mol kg}^{-1}.$$

Climatological values of PO<sub>4</sub><sup>\*</sup> attain a global maximum in the shelf waters of the Southern Ocean (these high values propagate to AABW during the formation process) and decrease gradually towards the north (Broecker et al., 1998), so reduced PO<sub>4</sub><sup>\*</sup> is a sensitive indicator of mixing with Scotia Sea waters. We observe a difference between the PO<sub>4</sub><sup>\*</sup> values of northward-flowing WSDW and those of southward-flowing WSDW, which has had access to lower-PO<sub>4</sub><sup>\*</sup> waters in the Scotia Sea (Fig. 6). At any given neutral density within the WSDW density class, PO<sub>4</sub><sup>\*</sup> is higher (by 0.05–0.1 μmol kg<sup>-1</sup>) over the deepest point and at the western side of each deep passage than at the eastern side. This difference is significantly larger than the precision of the measurements (0.02 μmol kg<sup>-1</sup>), and is apparent in the Orkney, Bruce, and Discovery Passages. In the Philip Passage, the bathymetry (and, in consequence, the deep flow) is more convoluted than farther east (Fig. 5) and the west–east asymmetry in the flow direction and properties of WSDW is not well-defined.

Fig. 4. Vertical distribution of the cross-track component of the LADCP velocity along the ALBATROSS South Scotia Ridge transect (above). Dark (white) shades denote northward (southward) flow. The contour interval is 5 cm s<sup>-1</sup>. Dashed lines represent the isopycnic water mass boundaries defined in Section 2.2. Station positions are marked in the lower axis. The deep Orkney Passage is expanded in the inset. Full-depth and WSDW cumulative transports along the section calculated from LADCP data (solid lines) and the LADCP-referenced geostrophic flow (broken lines) are shown in the lower panel.



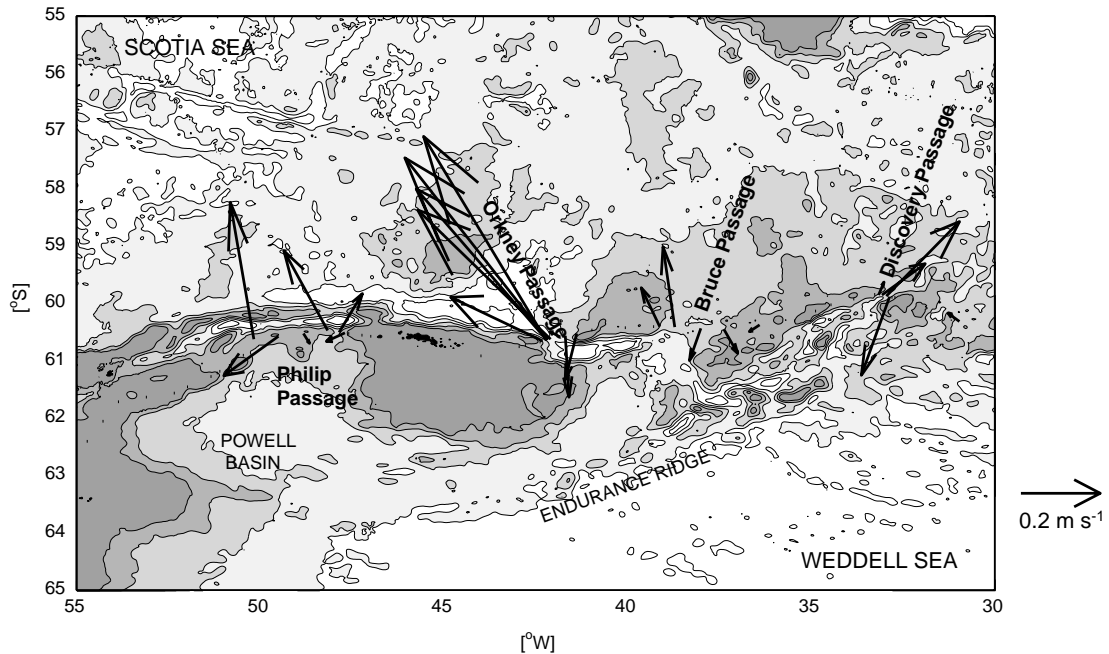


Fig. 5. Map of LADCp velocity vectors averaged over the WSDW density class along the ALBATROSS South Scotia Ridge transect. The bathymetry is from Smith and Sandwell (1997) and the contour interval is 1000 m.

With reinforced confidence in the LADCp record, we calculate the transport across the section in two ways: (1) directly from the water-track LADCp measurements; and (2) indirectly, by computing the geostrophic shear and estimating the barotropic component of the flow from the LADCp data. A least-squares fit of the geostrophic shear profile to the average water-track LADCp profile is performed at each station pair. For station pairs deeper than 200 m, LADCp measurements above this level are disregarded in the fit so as to exclude upper ocean ageostrophic motions. The fit is generally satisfactory, with a rms deviation (averaged over all station pairs) of  $4 \text{ cm s}^{-1}$  that arises principally from fine-scale vertical variability in the LADCp profiles. Large departures from geostrophy occur over the shallow topography west of Philip Passage, above the western flank of the South Orkney Plateau and within the narrow gap of Discovery Passage, but are sufficiently local so as not to raise concern about the general reliability of the referencing method. A further, subjective

adjustment of the geostrophic profile is nevertheless carried out in these regions by reference to the bottom-track LADCp record, which is expected to be more accurate than the water-track data over their common depth range. Flow through bottom triangles is accounted for in the transport calculations by extrapolating the deepest velocity value to the ocean floor at each station pair.

The cumulative transports quantified from methods (1) and (2) are displayed in Fig. 4. The full-depth LADCp transport amounts to  $27 \pm 7 \text{ Sv}$  ( $1 \text{ Sv} = 10^6 \text{ m}^3 \text{ s}^{-1}$ ), slightly higher than the  $22 \pm 7 \text{ Sv}$  yielded by the geostrophic estimate. The uncertainty in the transports is estimated here by applying random barotropic perturbations following a normal distribution with a standard deviation of  $3 \text{ cm s}^{-1}$  (the characteristic accuracy of the barotropic component of the LADCp flow, see Section 2.1) to individual velocity profiles, and calculating the rms deviation of 1000 realizations of the resulting transport. This assumes that the dominant source of error resides in the barotropic

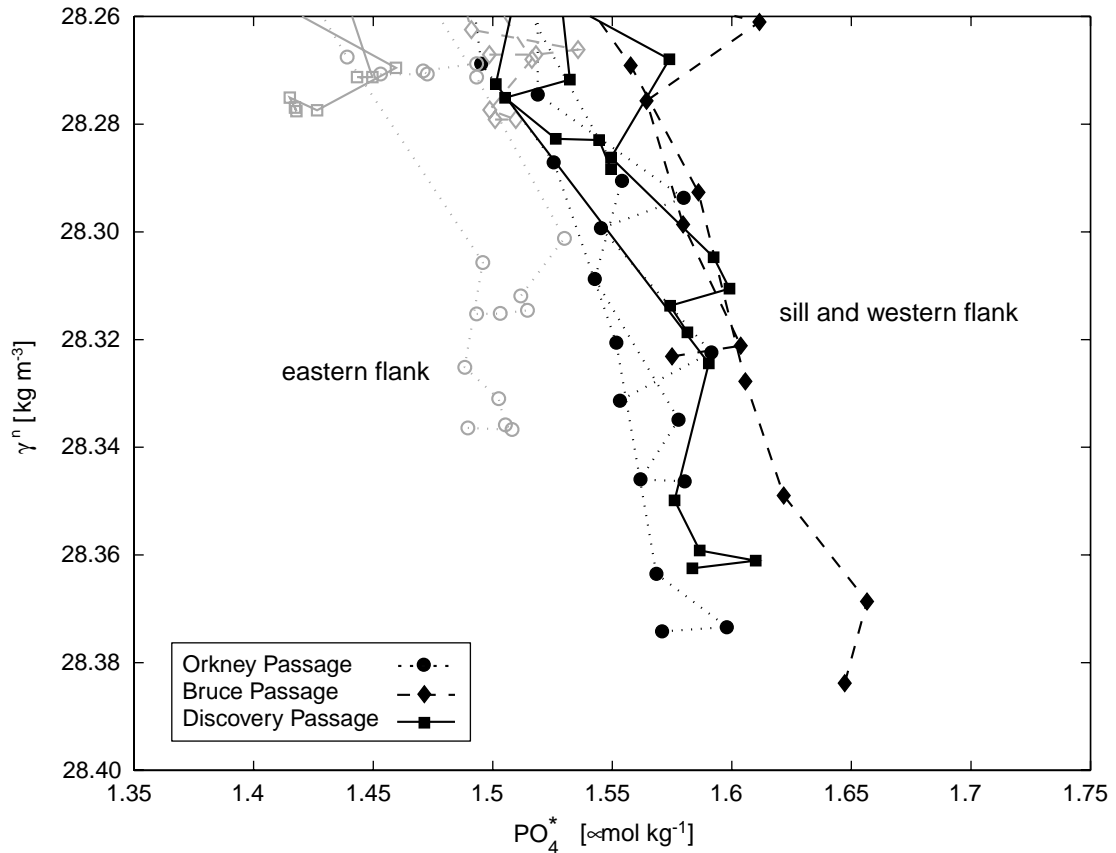


Fig. 6. Profiles of  $\text{PO}_4^*$  against neutral density in the Orkney, Bruce and Discovery Passages. Stations on the western flank and the sill (on the eastern flank) of each passage are shown in black (grey). Different symbols and line types are used for each passage.

component of the LADCP flow, and that errors are horizontally uncorrelated. Following Gordon et al. (2001), a different, ‘worst-case’ estimate of the error ( $\pm 18 \text{ Sv}$ ) can be obtained by assuming that all the LADCP profiles are systematically biased by  $1 \text{ cm s}^{-1}$  (the instrumental accuracy). Note, however, that none of these estimates include the sampling error due to the flow in the region of complex bathymetry west of the South Orkney Islands being poorly resolved, as indicated by the lack of spatial coherence in the velocity and  $\text{PO}_4^*$  measurements there. Approximately  $3 \text{ Sv}$  of the full-depth transport are effected in bottom triangles. Using a different bottom triangle formulation [in which the geostrophic velocity shear at the deepest common level is extrapolated down into the bottom triangle, and weighted by the ratio

of the squared buoyancy frequency of the deepest of each pair of stations to the squared buoyancy frequency at the deepest common level (Friedrichs, 1993)], yields a higher bottom triangle transport of  $6 \text{ Sv}$ . The regions at which the full-depth transport is most sensitive to the choice of bottom triangle formulation are the Bruce Passage and the rather shallow slope near  $35^\circ \text{W}$ , where high near-bottom velocities are observed and bottom triangles are large due to the wide station spacing. The geographical distribution of the full-depth transport (Fig. 4) is qualitatively similar for both methods (1) and (2), with major net contributions across the Antarctic Slope Front, the Orkney Passage, and the region of the Discovery Passage, and conspicuous localised reversals at the sill of the Orkney and Bruce Passages linked to the

dipolarity of the flow through each gap. The largest discrepancy between the two transport estimates occurs, not surprisingly, west of Philip Passage, where deviations of LADCP flow from geostrophy are most apparent and the sampling error may be large.

The net transport of WSDW over the South Scotia Ridge is, according to both calculations,  $6.7 \pm 1.7$  Sv (with a 'worst-case' error of  $\pm 2.6$  Sv), of which 2 Sv are transported in bottom triangles. The bulk of the WSDW transport ( $4.3 \pm 0.6$  Sv and  $6.0 \pm 0.6$  Sv from the LADCP and geostrophic computations, respectively) is concentrated in the Orkney Passage. The net transport of WSDW is barely distinguishable from zero in the Philip Passage ( $0.7 \pm 0.4$  and  $0.2 \pm 0.4$  Sv), the Bruce Passage ( $1.4 \pm 1.2$  and  $0.1 \pm 1.2$  Sv), and the Discovery Passage ( $0.5 \pm 0.2$  and  $0.4 \pm 0.2$  Sv). The choice of bottom triangle formulation affects the WSDW transport only minimally. The rate of WSDW export over the South Scotia Ridge calculated here represents a significant component of the AABW export from the Weddell Sea and is a factor of 4 larger than Locarnini et al.'s (1993) geostrophic estimate of 1.5 Sv for the Orkney Passage. Clearly, their assumption of zero flow at 1500 m is not applicable to the region, where we observe the flow to be equivalent barotropic.

#### 4. A box inverse model of the Weddell Sea

The model combines the ALBATROSS and WOCE A23 hydrographic sections assuming that they are representative of the mean state of the ocean and that the flow is in geostrophic balance (with a wind-driven Ekman contribution in the upper water column). It is initialised through the specification of a 'best guess' of the velocity field along each section, which is modified during the inversion so as to comply with the model's basic assumptions and a set of supplementary constraints. The rationale for our choice of initial velocity field is discussed in Section 4.1, with Section 4.2 presenting the details of the model. Section 4.3 describes the solution and its sensitivity to the various elements of the model.

##### 4.1. Initial velocity field

Along the ALBATROSS South Scotia Ridge transect we use the geostrophic flow calculated in Section 3 as the initial velocity field. During the WOCE A23 transect across the Weddell Gyre, however, direct velocity measurements were unavailable except at the crossing of the Antarctic Slope Front, where they were used by Heywood et al. (1998) to reference the local geostrophic flow. In the remainder of the transect, we base our initial estimate of the barotropic flow on in situ deep-current measurements collected by other expeditions. The rationale for our choice is explained in the following.

In the interior Weddell Gyre, north of the Antarctic continental slope ( $71.5^\circ\text{S}$ ) and south of the deep northern boundary current ( $62.5^\circ\text{S}$ ), we refer to the velocity measurements of the Weddell Gyre Study moored current-meter array (Fahrbach et al., 1994). A long-term, weak  $< 1 \text{ cm s}^{-1}$  interior cyclonic flow was revealed by the array near the ocean floor, with generally southwestward flow south of the gyre axis and northward flow northwest of the axis (following the cyclonic sense of the gyre, this is analogous to eastward flow north of the axis in WOCE A23). In the initialisation of the model, we express this as a westward (eastward) velocity of  $0.4 \text{ cm s}^{-1}$  south (north) of the gyre axis.

In a quasi-meridional LADCP section across the South Scotia Ridge near  $44^\circ\text{W}$ , Gordon et al. (2001) observe that the Endurance Ridge (Fig. 5) splits the deep boundary current of the northern Weddell Sea into two jets. One of these veers northward toward the Orkney and Bruce Passages, whereas the other continues to the east following the southern flank of the South Scotia Ridge. The southern core is detected again by Gordon et al. (2001) at  $40^\circ\text{W}$  and must feed the deep boundary current observed near  $31^\circ\text{W}$  in the WOCE A23 transect. Although some boundary current water is expected to leak northward across the region of Discovery Passage, we assume that the velocity structure of the current is modified little between  $40^\circ\text{W}$  and  $31^\circ\text{W}$ , and thus select the barotropic component of the geostrophic flow at this longitude to mimic Gordon et al.'s (2001)

Table 1  
Inverse model constraints ( $\pm$ estimated uncertainty) in the standard solution (a positive transport is northward/eastward)

Parameter	Value
Net mass flux into box	$0 \pm 2 \text{ Sv}$
Weddell Gyre transport	$40 \pm 5 \text{ Sv}$
Antarctic Slope Front transport on A23	$-14 \pm 3 \text{ Sv}$
Transport west of South Orkney Islands	$5 \pm 3 \text{ Sv}$
Net heat loss by the ocean	$15 \pm 8 \text{ W m}^{-2}$

observations. We use a reference velocity of  $4 \text{ cm s}^{-1}$  at 1500 m in the region where deep isopycnals shoal northward, and zero flow at the same depth in the region where the deep isopycnal slopes reverse, north of the 3500-m elevation at  $61.5^\circ\text{S}$ . Slightly further north, above the axis of the South Scotia Ridge, we assume zero bottom flow across the section, in accordance with LADCP measurements at neighbouring locations during ALBATROSS.

#### 4.2. The model

Our present oceanographic knowledge of the Weddell Sea is incorporated into the model in the form of five linear constraints, summarised in Table 1. Firstly, the net mass flux into the region is forced to be zero to within  $\pm 2 \text{ Sv}$ . This figure represents the uncertainty introduced by small contributions to the mass budget from the melting of ice shelves and icebergs, exchanges with the atmosphere, export of sea ice (these three are most probably trivial) and the asynopticity of the two sections.

From the Weddell Gyre Study current-meter array, Fahrbach et al. (1994) calculated that  $29.5 \pm 9.5 \text{ Sv}$  recirculate between Kapp Norvegia and the tip of the Antarctic Peninsula [this estimate was modified to  $34 \pm 2 \text{ Sv}$  by the variational assimilation scheme of Yaremchuk et al. (1998)]. A similar transport of  $28.3 \pm 8.1 \text{ Sv}$  was obtained by Muench and Gordon (1995) for the western boundary current [which accounts for about 90% of the gyre transport (Fahrbach et al., 1994)] near  $67.5^\circ\text{S}$ , using current-meter data from the Ice Station Weddell (ISW-1) and the geos-

trophic approximation. Further east, south of the South Scotia Ridge near  $44^\circ\text{W}$ , Gordon et al. (2001) measured a transport of about  $40 \text{ Sv}$  across the northern limb of the gyre. The most sophisticated numerical model of the Weddell Gyre to date (Beckmann et al., 1999) shows the annual-mean transport of the Weddell Gyre to increase eastwards from about  $30 \text{ Sv}$  near the western margin to more than  $50 \text{ Sv}$  at  $10^\circ\text{W}$ . The transport estimates above are thus in good agreement with the model diagnostics and, based on these, our second constraint sets the transport of the Weddell Gyre at the longitude of WOCE A23 to  $40 \pm 5 \text{ Sv}$ .

The third constraint follows from using two VMADCP transects across the southern end of the WOCE A23 section to estimate the geostrophic transport of the Antarctic Slope Front as  $14 \pm 3 \text{ Sv}$  (Heywood et al., 1998). From a current-meter array deployed in a nearby region, Fahrbach et al. (1992) demonstrated that there is a marked seasonal signal in the strength of the frontal current, with a maximum in austral autumn when the WOCE A23 survey was conducted. In order to account for a possible seasonal bias in Heywood et al.'s (1998) transport estimate, we increase the lower limb of the error bar in the constraint to  $5 \text{ Sv}$ .

In a LADCP transect across the Powell Basin, Gordon et al. (2001) observe a closed cyclonic circulation of  $18 \text{ Sv}$  in the region of the basin deeper than 2000 m. This suggests that the South Scotia Ridge overflow west of the South Orkney Islands is composed primarily of waters entering the Powell Basin from the south over the continental slope region shallower than 2000 m. The transport over this region immediately upstream of the Powell Basin is [according to the moored current-meter measurements of Fahrbach et al. (1994, 2001)]  $5 \text{ Sv}$ . This value corresponds closely to that derived from our LADCP-referenced geostrophic velocity field (Fig. 4) and forms the basis of our fourth constraint, setting the overflow transport west of the South Orkney Islands to  $5 \pm 3 \text{ Sv}$ . The importance of this constraint resides in its bounding of the mass and heat fluxes across a region where the sampling error is potentially large (see Section 3). The rather large uncertainty reflects the relatively low spatial resolu-

tion of Fahrbach et al.'s (1994, 2001) moorings, the possible deviation from a perfect closing of the 18 Sv cyclonic circulation in the deep Powell Basin, and entrainment of waters from the ACC regime or the Bransfield Strait. The existence of a substantial transport into the Powell Basin from the Bransfield Strait, however, is ruled out by observations (López et al., 1999; Gordon et al., 2000).

The fifth constraint allows the heat loss through the ocean surface within the inverse model domain to agree with recent estimates. In a coupled ocean/sea-ice model of the Weddell Gyre, Petit and Norro (2000) noted that the area-averaged oceanic heat flux fluctuates strongly on seasonal timescales, attaining a minimum of  $<5 \text{ W m}^{-2}$  in mid-summer, and a maximum of  $15\text{--}30 \text{ W m}^{-2}$  in autumn. This seasonality partly accounts for the variability present in in situ estimates of the oceanic heat flux. Based on the heat, salt, and oxygen budgets of the mixed layer, Gordon and Huber (1990) diagnosed an autumn value of  $41 \text{ W m}^{-2}$  and an annual value of  $16 \text{ W m}^{-2}$  for the Weddell Sea region near the Greenwich Meridian. For the same area but in late winter, McPhee et al. (1999) used a model of turbulent exchange at the ice-ocean interface to calculate a mean oceanic heat flux of  $27 \text{ W m}^{-2}$  during the drift of a buoy equipped with an array of temperature and conductivity sensors. Fahrbach et al. (1994) estimated that  $19 \text{ W m}^{-2}$  must be lost from the ocean to balance the heat converging into the oceanic region south of the Weddell Gyre Study current-meter array [this estimate was modified to  $15 \text{ W m}^{-2}$  by the variational assimilation scheme of Yaremchuk et al. (1998)]. Similarly, Martinson (1994) estimated an average oceanic heat flux of  $19 \text{ W m}^{-2}$  over the gyre from the observed fields of ice thickness and divergence. In their study of ocean bulk property distributions in the Weddell Gyre, Martinson and Iannuzzi (1998) inferred that the oceanic heat flux, averaged over the 5 months of the cooling season, is  $25\text{--}35 \text{ W m}^{-2}$  throughout much of the gyre. Maximum spatial variations in this quantity were small ( $\sim 30\%$ ) despite vast regional changes in stratification and dynamical setting. They pointed out, however, that the applicability of their result near the perennially ice-covered continental slope re-

gion of the western Weddell Sea is doubtful. There, Robertson et al. (1995) estimated an ice-ocean (autumn) heat flux of  $1.7 \text{ W m}^{-2}$  from microstructure measurements gathered during the ISW-1. For the same location and period, Lytle and Ackley (1996) obtained an oceanic heat flux of  $7 \pm 2 \text{ W m}^{-2}$  by combining a heat flux model of the sea ice with the data from an array of thermistors deployed in the ice.

Our choice of  $15 \pm 8 \text{ W m}^{-2}$  is roughly centred within the above range of values and encompasses all annual and long-term estimates. One could argue that, with a substantial area of the inverse model domain being perennially ice-covered, this figure should be slightly reduced to reflect the smaller heat flux there. In this respect we note the compensating effect of the continental margin processes associated with polynyas and ocean-ice shelf interaction, which are not included in either Robertson et al.'s (1995) or Lytle and Ackley's (1996) estimates. With a model area of  $2.1 \times 10^{12} \text{ m}^2$ ,  $15 \pm 8 \text{ W m}^{-2}$  is equivalent to an oceanic heat (potential temperature) transport into the domain of  $3.1 \times 10^{13} \pm 1.6 \times 10^{13} \text{ W}$  ( $7.5 \times 10^6 \pm 3.8 \times 10^6 \text{ K s}^{-1}$ ).

The five model layers were bounded by the neutral density surfaces defined in Section 2.2. The resulting system of five equations (corresponding to each of the constraints) and 85 unknowns (the barotropic velocities at each of the station pairs in the two sections) was set up as a matrix equation using version 4.2 of DOBOX (Morgan, 1994) and solved through singular value decomposition (Wunsch, 1996). Each column of the matrix was weighted by the typical uncertainty in the initial estimate of the barotropic velocity at its corresponding station pair, and normalised by the station pair area. Selected uncertainties were  $4 \text{ cm s}^{-1}$  for stations over the South Scotia Ridge or within the southern crossing of the Antarctic Slope Front,  $1 \text{ cm s}^{-1}$  in the interior Weddell Gyre, and  $8 \text{ cm s}^{-1}$  in the boundary current just south of the South Scotia Ridge. Since we used the full rank (rank 5) solution, no row scaling was applied. The wind-driven Ekman transport across each section was calculated from the Hellerman and Rosenstein (1983) annual mean wind stress climatology (assuming an Ekman depth of 60 db) and assigned

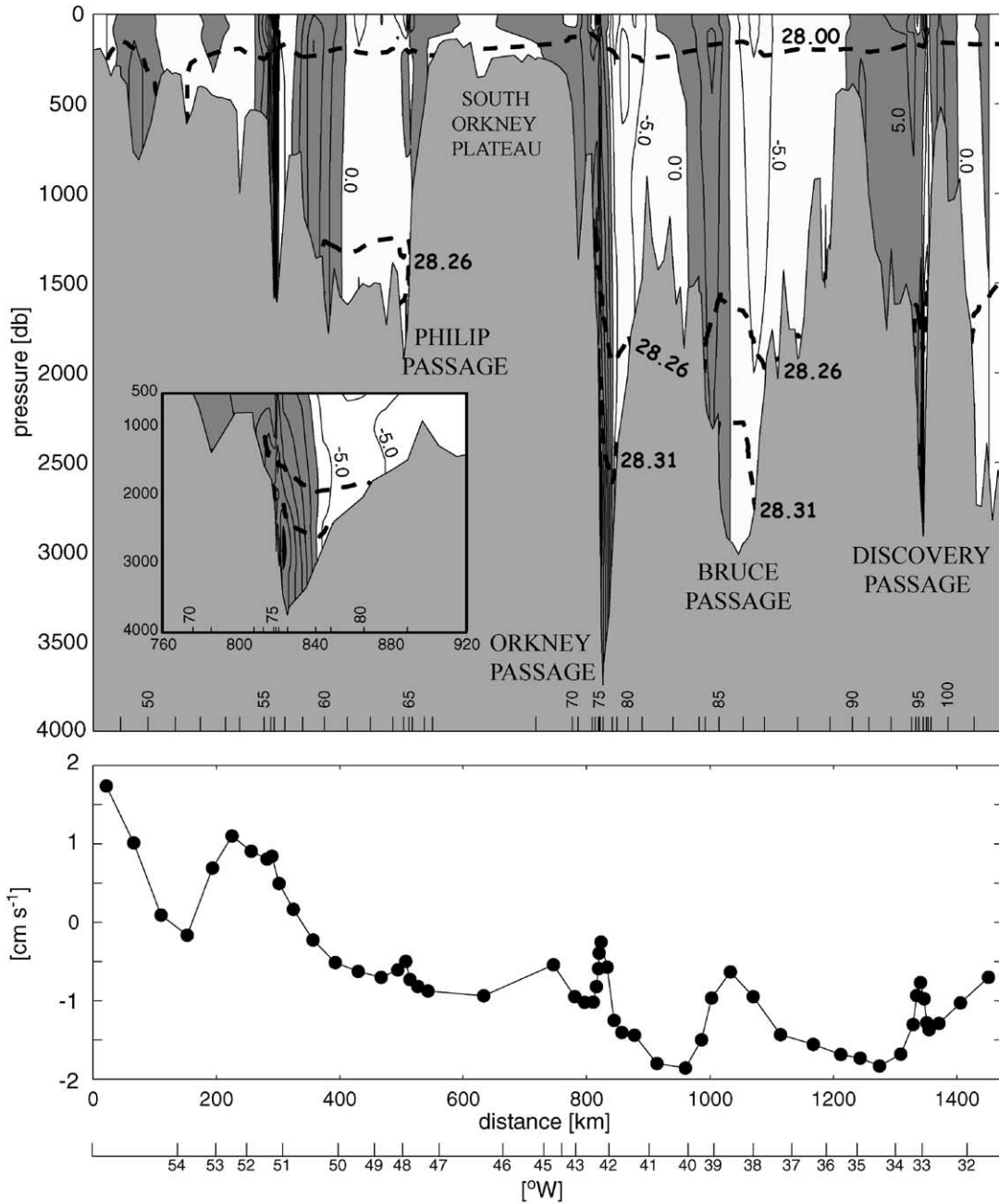


Fig. 7. Vertical distribution of the geostrophic velocity of the solution along the ALBATROSS South Scotia Ridge transect (above). Dark (white) shades denote northward (southward) flow. The contour interval is  $5 \text{ cm s}^{-1}$ . Dashed lines represent the isopycnal water mass boundaries defined in Section 2.2. The deep Orkney Passage is expanded in the inset. The adjustment to the initial velocity field is displayed in the lower panel.

to the shallowest layer in the model. The net Ekman transport was of 0.6 Sv directed out of the model domain, as expected from the divergent wind field over the interior Weddell Gyre. The bulk of this transport (0.55 Sv) was effected northward across the South Scotia Ridge.

In the model, we treat station 37 of WOCE A23 as the northern end of the subsection instead of station 35 ( $0.5^\circ$  to the south) where WOCE A23 converges with ALBATROSS (Fig. 1). In 1999 the Southern Boundary of the ACC was located  $0.5^\circ$  further south than in 1995 and deep isopycnals in the region of the South Scotia Ridge were depressed (Meredith et al., 2001a), so by using station 37 we aim to mitigate the impact of interannual variability on the model's solution. The effect of this is assessed below.

#### 4.3. Solution

The velocity field of the solution over the South Scotia Ridge (Fig. 7) strongly resembles the initial field (Fig. 4), with a mean (maximum) absolute difference of 1.0 (1.9)  $\text{cm s}^{-1}$ . West of about  $50^\circ\text{W}$ , the velocity is generally increased (i.e. more northward), whereas east of that longitude it is reduced throughout. Superimposed on this background pattern, the solution, though negative, attains a local maximum in each of the deep passages. These features of the solution arise from the oceanic heat-flux constraint. Cold waters west of the Antarctic Slope Front and in the deep passages are forced northward, enhancing the oceanic heat convergence in the box to balance the surface heat loss (in the initial field, the oceanic heat-flux into the box is equivalent to a heat gain by the ocean of  $3 \text{ W m}^{-1}$ , i.e. it has the wrong sign).

Along the WOCE A23 section, the mean absolute difference between the initial velocity field and that of the solution is merely  $0.4 \text{ cm s}^{-1}$  (Fig. 8). The largest positive (i.e. eastward) velocity adjustment is applied by the model over the upper continental slope south of  $72^\circ\text{S}$  (exceeding  $3.5 \text{ cm s}^{-1}$ ) and within the deep boundary current near  $62^\circ\text{S}$  (reaching  $1.8 \text{ cm s}^{-1}$ ). By increasing the transport of the deep boundary current, which conveys relatively cold waters, the solution again

acts to increase the oceanic heat convergence in the box. In the interior Weddell Gyre, the model adds an eastward velocity of about  $0.15 (0.03) \text{ cm s}^{-1}$  to the southern (northern) limb of the gyre to adjust the transport (initially 45 Sv) to the 40 Sv specified in the constraints. Note that although salt conservation was not enforced as a constraint, the net salt transport into the model domain is not significantly different from zero in the solution, as is expected from the measured sea-ice export from the Weddell Sea (Harms et al., 2001).

As the system of equations is heavily under-determined, the model solution is very sensitive to the initial specification of the flow field, of which we claim to know the direction and approximate magnitude (within a typical uncertainty prescribed in the column weighting). To a far lesser extent, the solution is also dependent on the Ekman transport. Calculating the Ekman fluxes from annual mean reanalysis wind-stress fields from the European Centre for Medium Range Weather Forecast (ECMWF) (Trenberth et al., 1989) instead of the Hellerman and Rosenstein (1983) climatology used in the standard run yields a reduced net Ekman transport out of the model domain of 0.16 Sv (cf. 0.6 Sv in the standard run). This is achieved through an increased westward Ekman flux across WOCE A23 of 0.35 Sv (cf. 0.05 Sv in the standard run), with the northward Ekman transport over the South Scotia Ridge remaining close to 0.5 Sv. The impact of the above changes on the water mass budgets of the solution is, however, small in comparison with that of the uncertainties in the constraints (Table 2).

The sensitivity of the model's outcome to these uncertainties was assessed by exploring the parameter space, altering one constraint at a time by its expected error. By far the largest uncertainty in the results is introduced by the oceanic heat-flux constraint (Table 2). This is as expected from both a relatively large error bar and the causal relationship linking the oceanic heat flux to ocean stability, which controls water-mass transformations in the Weddell Sea (Martinson and Iannuzzi, 1998). For example, increasing the heat flux to  $23 \text{ W m}^{-2}$  is conducive to an enhanced transformation of AASW and WDW to AABW at a rate of 13.0 Sv (cf. 9.7 Sv in the standard solution)

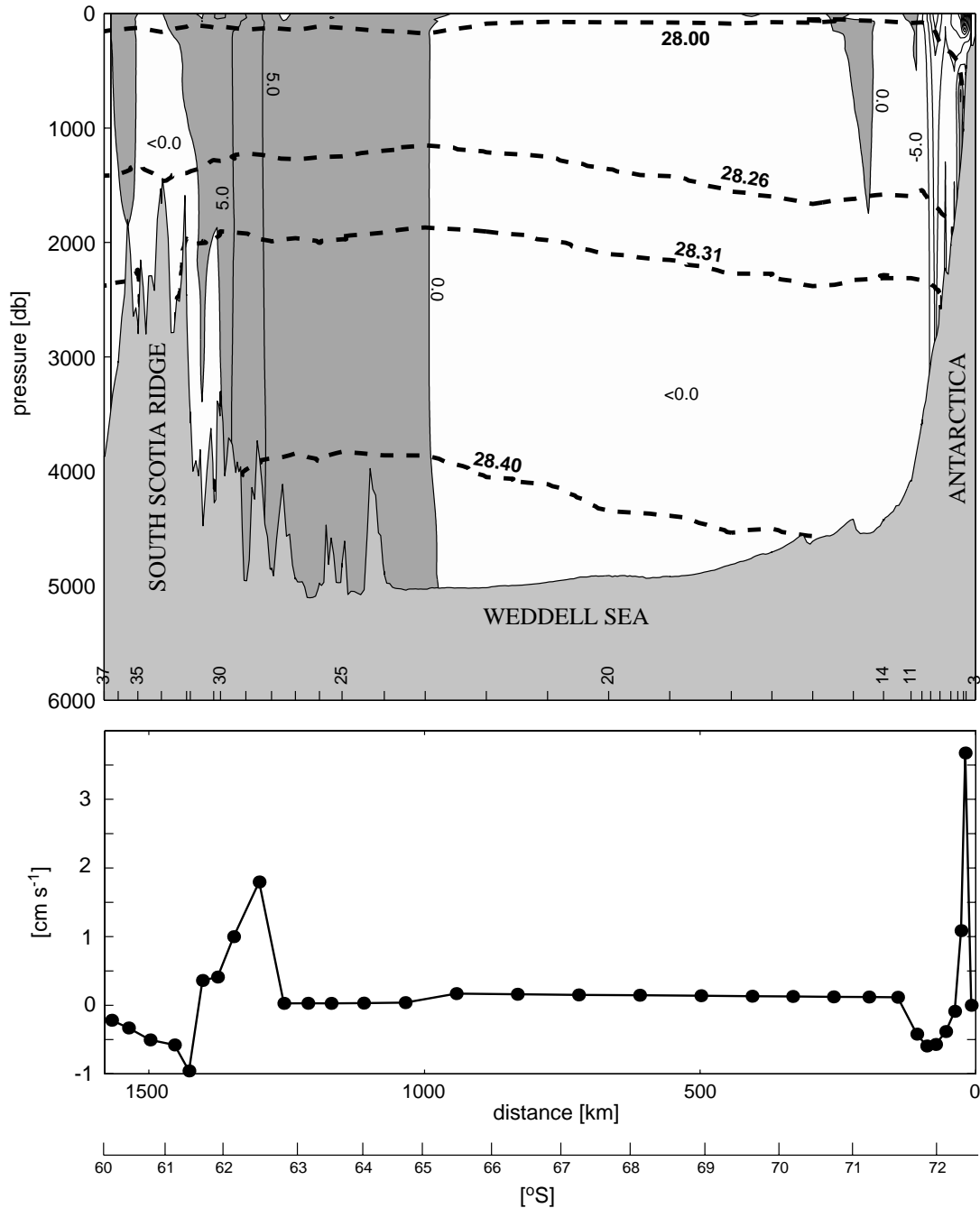


Fig. 8. Vertical distribution of the geostrophic velocity of the solution along the WOCE A23 crossing of the Weddell Sea (above). Dark (white) shades denote eastward (westward) flow. The contour interval is  $5 \text{ cm s}^{-1}$ . Dashed lines represent the isopycnal water mass boundaries defined in Section 2.2. The adjustment to the initial velocity field is displayed in the lower panel.

Table 2

Water mass budget (in Sv) of the solution for each model run (a positive transport is northward/eastward) The details of each sensitivity test are given in Section 4.3.

Parameter	Value	AASW	WDW	WSDW	WSBW
<i>Standard</i>		−1.7	−8.0	5.8	3.9
Ekman transport from ECMWF winds		−2.2	−8.2	6.4	4.0
Net mass flux out of the box	−2 Sv	−1.8	−9.0	5.0	3.8
	2 Sv	−1.6	−7.0	6.6	4.0
Weddell Gyre transport	35 Sv	−1.9	−8.1	6.0	4.0
	45 Sv	−1.6	−7.8	5.6	3.8
Antarctic Slope Front Transport on A23	−9 Sv	−1.4	−7.4	5.3	3.5
	−17 Sv	−1.9	−8.3	6.1	4.1
Transport west of South Orkney Islands	2 Sv	−2.3	−8.6	6.9	4.1
	8 Sv	−1.1	−7.3	4.7	3.7
Net heat loss by the ocean	7 W m <sup>−2</sup>	−1.3	−5.0	3.2	3.2
	23 W m <sup>−2</sup>	−2.1	−10.9	8.4	4.6
Northernmost A23 station	35	−2.2	−8.4	6.6	4.0
	40	−1.6	−7.8	5.4	3.9

whereas decreasing the heat flux to 7 W m<sup>−2</sup> leads to a reduced transformation of 6.3 Sv.

In comparison, uncertainties in the other constraints lead to water-mass transformation rates that deviate from the standard solution by about a third of the deviation due to oceanic heat-flux errors. Thus, setting the overflow transport west of the South Orkney Islands to 2 and 8 Sv results in an AABW formation rate of 11.0 and 8.4 Sv, respectively. A smaller overflow transport reduces the model's ability to satisfy the oceanic heat-flux constraint by flushing cold water over the western sector of the South Scotia Ridge. To overcome the ensuing heat imbalance, the model increases the transport of the deep boundary current in the northern Weddell Sea and, in doing so, fosters AABW export.

A value of 8.8 (10.2) Sv is obtained by forcing the transport of the Antarctic Slope Front in the WOCE A23 section to 9 (17) Sv. The model's response to a reduced frontal transport (and the associated diminished oceanic heat flux into the box) is to expel more relatively cold water over the eastern sector of the South Scotia Ridge and in the deep boundary current of the northern Weddell Sea, enhancing the AABW export and pumping more heat into the box. Less intuitive is the model's behaviour when the Weddell Gyre trans-

port is altered to 35 and 45 Sv, leading to respective AABW formation rates of 10.0 and 9.4 Sv. That the greater gyre transport produces a smaller AABW export is a complex result of the meridional evolution of the AABW layer thickness and the need to comply simultaneously with the net mass and oceanic heat-flux constraints.

An additional test was conducted to examine the sensitivity of the model output to the choice of the northernmost WOCE A23 station used in the model. We ran the model with stations 35 and 40 (Fig. 1) as the northern end of the subsection, the former corresponding to the geographical convergence of WOCE A23 and ALBATROSS. The impact of these modifications on the water mass budgets produced by the model is small (Table 2), with AABW formation rates of 10.6 Sv (station 35) and 9.3 Sv (station 40). Using station 35, the oceanic heat flux in the initial field is further biased out of the box, contrary to what would be expected from measurements of the oceanic heat flux in the Weddell Sea but qualitatively consistent with the interannual changes observed by Meredith et al. (2001a). Not only did they report an apparent southward shift of the Southern Boundary of the ACC and the density field between 1995 and 1999 (which is accounted for by our choice of station 37 as the northernmost station in the

standard solution), but diagnosed a general warming (by about  $0.1^{\circ}\text{C}$ ) of the WDW layer over the South Scotia Ridge.

To estimate the effect of this warming on the solution, we artificially imposed a cooling of  $0.1^{\circ}\text{C}$  throughout the WDW layer over the South Scotia Ridge while preserving the original layer structure and geostrophic shear of the water column. As a result the oceanic heat flux in the initial field (scaled as an equivalent heat flux through the ocean surface) shifted from approximately 3 to  $4\text{ W m}^{-2}$  (heat gained by the ocean). This change had no significant impact on the outcome of the inversion due to the original layer structure and shear being preserved. The magnitude and sign of the change indicate that the initial imbalance in the heat budget does probably not arise from the asynopticity of the sections but from errors in the initial velocity field.

Below, we will assume that velocity errors are well represented by the model's column weighting, and that any errors due to the asynopticity of the sections not captured by the extension to WOCE A23 station 37 are reflected in the error bar of the net mass flux constraint. We will thus regard the uncertainty in the model diagnostics as arising purely from uncertainties in the constraints, and estimate the former as a quadratic sum of the errors introduced by each of the latter.

## 5. Discussion

Over the South Scotia Ridge, the transport curve associated with the box inverse model solution (Fig. 9a) broadly preserves the observed shape (Fig. 4), but the relative strength of northward and southward flows has been modulated to produce a net full-depth overflow transport of  $7 \pm 6\text{ Sv}$ , smaller than the original  $22 \pm 7\text{ Sv}$ . West of the South Orkney Islands, most of the transport is effected by the Antarctic Slope Front system (about  $7\text{ Sv}$  in both the solution and the observations), part of which returns southward further east in a flow that may be coupled to the cyclonic circulation prevailing in the Powell Basin. On the western flank of the Orkney Passage, a northward flow of about  $12\text{ Sv}$  is apparent in both the

LADCP-referenced geostrophic transport and the solution that must feed the  $10\text{ Sv}$  westward jet observed by Gordon et al. (2001) northeast of the South Orkney Islands, and which compares closely with the full-depth Orkney Passage transport of  $9\text{ Sv}$  obtained by Matano et al. (2002) in a numerical study. A total of  $7\text{ Sv}$  in the solution ( $5\text{ Sv}$  in the observations) are transported to the south over the eastern flank of the Orkney Passage, with  $5\text{ Sv}$  ( $8\text{ Sv}$  in the observations) flowing northward over the western side of Bruce Passage. One of the main differences between the solution and the observed transports occurs in the eastern region of Bruce Passage, where an observed southward transport of  $9\text{ Sv}$  is augmented to  $13\text{ Sv}$  in the solution. Further east, through Discovery Passage, the model decreases the observed northward transport of  $9$  to  $5\text{ Sv}$ . Across the WOCE A23 section (Fig. 9b), the Weddell Gyre transports  $40\text{ Sv}$  westward south of its axis at  $65^{\circ}\text{S}$ . Of these,  $33\text{ Sv}$  recirculate eastward south of the South Scotia Ridge, with the remainder overflowing the ridge. The northern boundary current, where the uncertainty in the initial velocity field was greatest, transports  $25\text{ Sv}$ . This value agrees well with that measured by Gordon et al. (2001) in the same boundary current south of the Endurance Ridge at  $40^{\circ}\text{W}$ .

The model diagnoses that  $4.7 \pm 0.7\text{ Sv}$  of WSDW are fluxed over the South Scotia Ridge (Fig. 9a), less than the  $6.7 \pm 1.7\text{ Sv}$  derived from the observations. The distribution of the transport amongst passages remains similar, with the bulk flowing through the Orkney Passage ( $5.6 \pm 0.1\text{ Sv}$ ) and minor contributions from the other gaps ( $-0.1 \pm 0.3\text{ Sv}$  from the Philip Passage;  $-0.7 \pm 0.3\text{ Sv}$  from the Bruce Passage and  $0.2 \pm 0.1\text{ Sv}$  from the Discovery Passage). The magnitude and distribution of these transports are in broad agreement with those in the numerical simulation of Schodlok et al. (2002), who report a WSDW export over the ridge of  $6.4\text{ Sv}$  concentrated in the Orkney Passage ( $4.2\text{ Sv}$ ). The main disagreement between their model and our results concerns the WSDW transport through Philip Passage, which they quantify as  $2.2\text{ Sv}$ . Our diagnosed WSDW transport over the ridge continues to be substantially larger (by a factor of 3) than the geostrophic

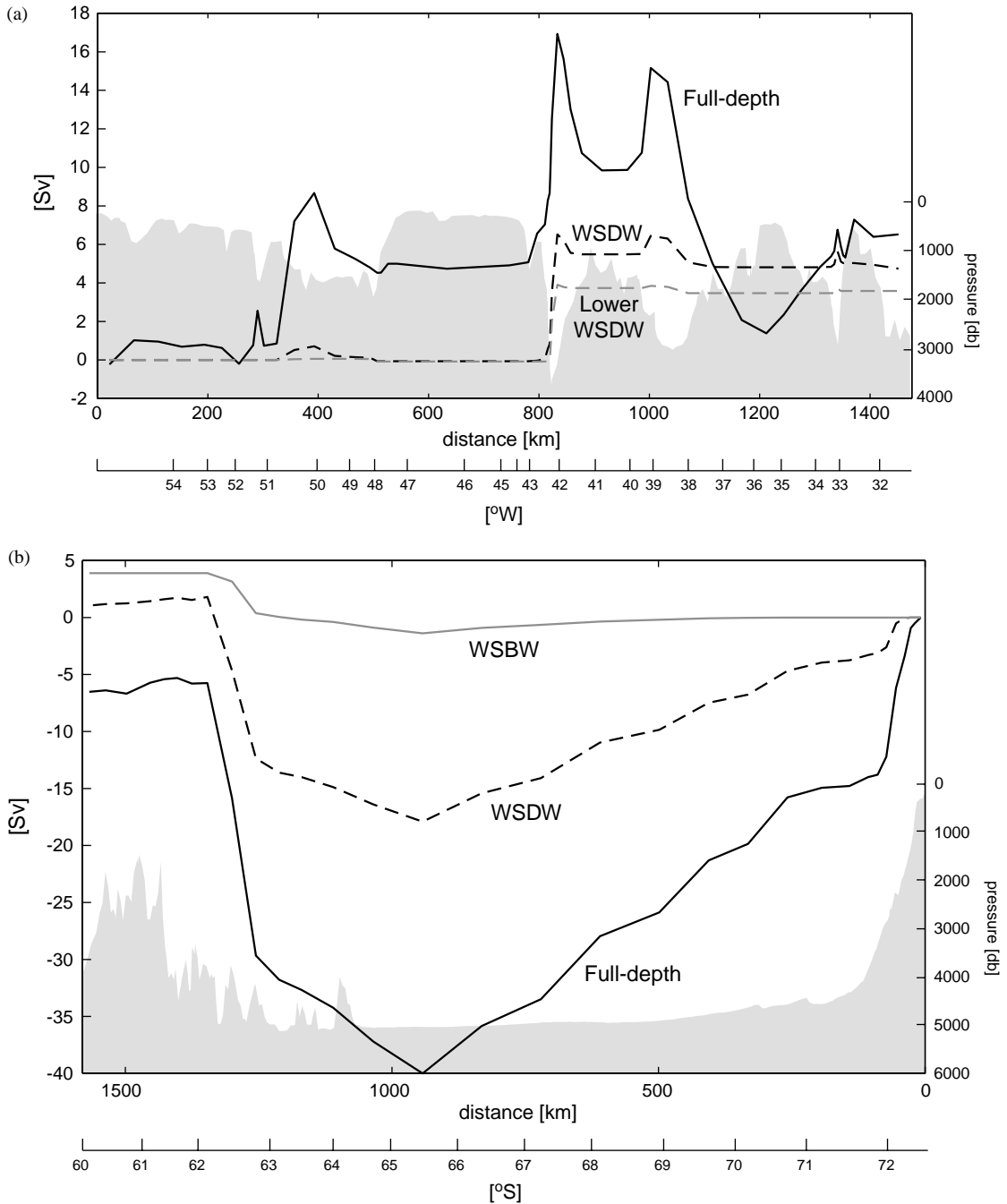


Fig. 9. Cumulative transport curves associated with the solution along the ALBATROSS South Scotia Ridge transect (a) and the WOCE A23 crossing of the Weddell Gyre (b). The solid, black dashed and grey dashed lines in (a) represent full-depth, WSDW and LWSDW transports, respectively. The solid, dashed and grey lines in (b) show full-depth, WSDW and WSBW transports. The bottom topography is indicated by the shaded region.

estimate of Locarnini et al. (1993) for the Orkney Passage. South of the ridge, the northern limb of the Weddell Gyre transports 20 Sv of WSDW and 5 Sv of WSBW (Fig. 9b). These values compare well with LADCP transport estimates by Gordon et al. (2001) at 44°W, where 25 Sv of WSDW and 5 Sv of WSBW flow eastwards in the northern limb of the gyre (Schodlok et al., 2002, obtained nearly identical values in their numerical study). As the location of their section lies slightly upstream of the Orkney Passage, some WSDW (about 5–6 Sv according to our observations and the model solution) will leave the gyre before reaching the WOCE A23 section, thereby accounting for the reduced WSDW transport there. The circulation of AABW in the western Weddell Gyre as diagnosed by the model is schematised in Fig. 10.

The deviations of the transports output by the model from the LADCP-referenced geostrophic values have been achieved through perturbations to the velocity field that are well within the expected velocity errors. With no other evidence

to hand, it is difficult to ascertain whether the model solution over the South Scotia Ridge is closer to the true ‘steady-state’ (averaged over several annual cycles) component of the transport field than the observed snapshot. We now investigate this issue by examining the compatibility of the observed transports with our previous oceanographic knowledge of the Weddell Sea (as synthesised by the model’s constraints). We run the model with two additional constraints setting the South Scotia Ridge full-depth and WSDW overflow transports to their observed geostrophic values of  $22 \pm 7$  and  $6.7 \pm 1.7$  Sv. The solution suggests that in order to satisfy all seven constraints a westward transport of 17 Sv (9 Sv in the WSDW layer) is required across the WOCE A23 segment north of 62°S. This is achieved through westward bottom velocities of  $2\text{--}7\text{ cm s}^{-1}$  and implies that a major fraction of the northern boundary current of the Weddell Sea recirculates immediately to the east of the section and provides a dominant contribution to the South Scotia Ridge

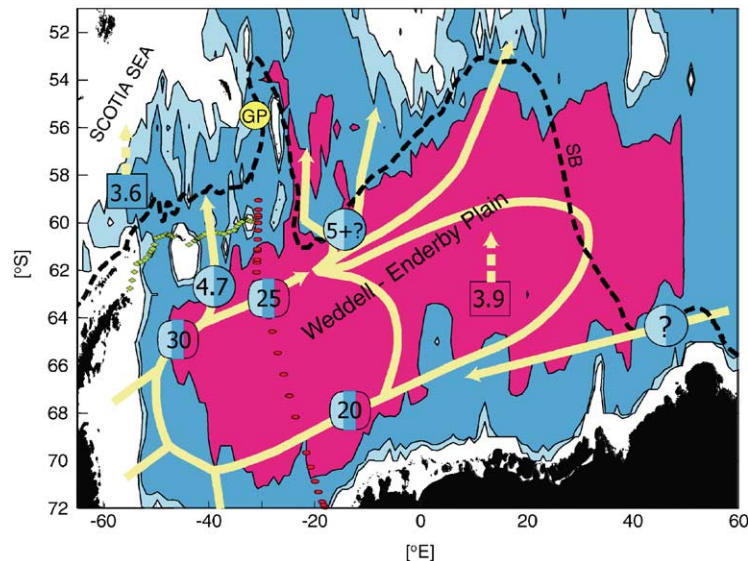


Fig. 10. Bottom neutral density from the WOCE 1998 climatology in three classes: Upper WSDW (light blue), Lower WSDW (dark blue) and WSBW (magenta). ALBATROSS and WOCE A23 station positions are indicated by the green diamonds and red ellipses, respectively. Georgia Passage (GP) is marked by the yellow circle and the Southern Boundary of the ACC (SB) by the thick dashed line. The circulation of AABW in the region as diagnosed by the inverse model is schematised by the arrows. Transports (in Sv) are shown by the circled figures, and the AABW classes involved are denoted by the colours of the circles. The squares and associated dashed arrows represent upward entrainment, also given in Sv. The model assumes that the unknown input of AABW from the Indian sector (indicated by a question mark) is zero.

overflow. A westward flow of such magnitude is not reflected in any of the direct velocity measurements available in the region (which indicate that the flow over the ridge is fed primarily from the west) and so the observed geostrophic transports over the ridge (particularly the full-depth one) seem too large to be consistent with the model constraints. Although errors in the observed transports (especially the sampling error) or the constraints may be important, temporal variability in the transports is likely to contribute to the inconsistency. Indeed, the deep current field south of the South Scotia Ridge and the Weddell Gyre transport have been shown to fluctuate on seasonal timescales, with relatively high values in the season of the ALBATROSS South Scotia Ridge transect (Barber and Crane, 1995; Beckmann et al., 1999; Fahrbach et al., 2001; Schodlok et al., 2002).

In the standard solution, the western Weddell Gyre transforms  $1.7 \pm 0.8$  Sv of AASW and  $8.0 \pm 3.2$  Sv of WDW into  $5.8 \pm 3.0$  Sv of WSDW and  $3.9 \pm 0.8$  Sv of WSBW (totalling  $9.7 \pm 3.7$  Sv of AABW). Estimates of AABW production in the Weddell Sea to date are listed in Table 3 for comparison. Many of these estimates have been limited to the WSBW layer and obtained through quantification of the WSBW transport in the western boundary current of the gyre. Our WSBW formation rate of  $3.9 \pm 0.8$  Sv lies within the range of those values (1–5 Sv) and agrees closely with several of them. The WSBW transport curve in Fig. 9b suggests that this is due to the net WSBW production and the WSBW transport of the boundary current being essentially identical, as expected since the bulk of the newly produced WSBW is channelled into the boundary current. Several other estimates of WSBW production based on natural and anthropogenic tracer budgets or integrated measurements of the gyre transport (Fahrbach et al., 1994; see also the variational assimilation analysis of Yaremchuk et al., 1998) are also in broad agreement with our model's diagnostics. Given the variety of WSBW definitions and uncertainties involved, the WSBW production estimates listed in Table 3 can rarely be considered to differ significantly from our result (to facilitate comparison with other studies, our

diagnosed AABW and WSBW production rates corresponding to a number of water mass definitions are shown). We note, however, that in the sensitivity tests in Table 2 the WSBW production rate never approaches values as low as 1.3 Sv (Fahrbach et al., 2001) or 2 Sv (Foldvik et al., 1985). The nature of these two works suggests that they may not have captured a substantial portion of the newly formed WSBW.

As illustrated by Table 3, there have been fewer attempts at estimating the total AABW production in the Weddell Sea, and the results span a wide range of values. The lower end, near 4 Sv, is shared by Fahrbach et al. (1994), Yaremchuk et al. (1998), the chlorofluorocarbon-based estimate of Orsi et al. (1999) and the lower estimates of Weiss et al. (1979) and Meredith et al. (2001b), whereas Gill (1973), Carmack (1977), the mass budget analysis of Orsi et al. (1999) and the upper estimates of Weiss et al. (1979) and Meredith et al. (2001b) give somewhat higher rates approaching 6–8 Sv. Our  $9.7 \pm 3.7$  Sv is closest to the 11 Sv of Mensch et al. (1997), Sloyan and Rintoul (2001) and Hellmer and Beckmann (2001), at the upper end of the range. The absence of a clear dependency of the calculated rate on the method suggests that much of this variability can possibly be ascribed to differing AABW definitions, inter-annual changes and, mainly, estimation errors. In the framework of our model, AABW production rates below 6.4 Sv appear to be inconsistent with present estimates of the oceanic heat flux in the western Weddell Sea. For example, in order to produce only 4.5 Sv of AABW (a scenario suggested by several of the AABW production estimates in Table 3) while preserving a reasonable transport function (here 'reasonable' means compatible with the mass transport constraints in Table 1), the model requires an imposed oceanic heat flux as low as  $3 \text{ W m}^{-2}$ , which is in disagreement with values in the literature (see Section 4.2). Although a solution exists in which 4.5 Sv of AABW are formed and  $15 \text{ W m}^{-2}$  are liberated through the ocean surface (as in the standard solution), this involves a reduction of the transport of the deep boundary current in the northern Weddell Sea that leads to a near-zero AABW export east of the Scotia Sea, in clear conflict with

Table 3

Estimates of AABW and WSBW production rates (in Sv) in the Weddell Sea [adapted from Orsi et al. (1999)]

Source	Water mass	Production rate
<i>Deep Boundary Current transport</i>		
Carmack and Foster (1975)	WSBW ( $-1.4 < \theta < -1.2^\circ\text{C}$ )	2–5
Foster and Carmack (1976)	WSBW ( $\theta = -1.3^\circ\text{C}$ )	3.6
Foldvik et al. (1985)	WSBW ( $\theta = -0.8^\circ\text{C}$ )	2
Gordon et al. (1993)	WSBW ( $\theta < -0.8^\circ\text{C}$ )	3
Fahrbach et al. (1995)	WSBW ( $\theta < -0.7^\circ\text{C}$ )	1–4
Muench and Gordon (1995)	WSBW ( $\theta < -0.8^\circ\text{C}$ )	2.5–3
Gordon (1998)	WSBW ( $\theta = -1.1^\circ\text{C}$ , $\theta < -0.7^\circ\text{C}$ )	3–4
Fahrbach et al. (2001)	WSBW ( $\theta < -0.7^\circ\text{C}$ )	$1.3 \pm 0.4$
<i>Weddell Gyre transport</i>		
Fahrbach et al. (1994)	AABW ( $\theta < 0^\circ\text{C}$ )	3.3–5.6
	WSBW ( $\theta < -0.8^\circ\text{C}$ )	2.6–2.8
<i>Shelf Water budgets</i>		
Gill (1973)	AABW ( $\theta = -0.6^\circ\text{C}$ )	6–9
Carmack (1977)	AABW ( $\theta < 0^\circ\text{C}$ )	5–10 <sup>a</sup>
<i>Natural and anthropogenic tracers</i>		
Weiss et al. (1979)	AABW ( $\theta = -0.4^\circ\text{C}$ )	4.5, 8
	WSBW ( $\theta = -0.9^\circ\text{C}$ )	3, 5
Weppernig et al. (1996)	WSBW ( $\theta = -0.7^\circ\text{C}$ )	5
Mensch et al. (1997)	AABW ( $\theta = -0.5^\circ\text{C}$ )	11
	WSBW ( $\theta = -1.0^\circ\text{C}$ )	3.5
Orsi et al. (1999)	AABW ( $\gamma^n > 28.27 \text{ kg m}^{-3}$ )	8.1 <sup>a</sup>
Meredith et al. (2001b)	AABW ( $\theta < 1.0^\circ\text{C}$ )	$< 6.6$ , $3.7 \pm 1.6$
<i>Mass budget</i>		
Orsi et al. (1999)	AABW ( $\gamma^n > 28.27 \text{ kg m}^{-3}$ )	10 <sup>a</sup>
<i>Freshwater budget</i>		
Harms et al. (2001)	WSBW ( $\theta < -0.7^\circ\text{C}$ , $S > 34.64$ )	2.6
<i>Numerical models</i>		
Hellmer and Beckmann (2001)	AABW ( $\sigma_2 > 37.16 \text{ kg m}^{-3}$ )	11
<i>Inverse models</i>		
Yaremchuk et al. (1998)	WSDW ( $-0.8 < \theta < 0^\circ\text{C}$ )	$2.6 \pm 1.3$
Sloyan and Rintoul (2001)	WSBW ( $\theta < -0.8^\circ\text{C}$ )	$2.5 \pm 1.9$
This study	AABW ( $\gamma^n > 28.30 \text{ kg m}^{-3}$ )	$11 \pm 1$
	AABW ( $\gamma^n > 28.26 \text{ kg m}^{-3}$ )	$9.7 \pm 3.7$
	( $\theta < 0^\circ\text{C}$ )	$10.0 \pm 3.7$
	( $\gamma^n > 28.27 \text{ kg m}^{-3}$ )	$9.8 \pm 3.7$
	( $\sigma_2 > 37.16 \text{ kg m}^{-3}$ )	$9.8 \pm 3.7$
	( $\gamma^n > 28.30 \text{ kg m}^{-3}$ )	$10.2 \pm 3.8$
	WSBW ( $\gamma^n > 28.40 \text{ kg m}^{-3}$ )	$3.9 \pm 0.8$
	( $\theta < 0.7^\circ\text{C}$ )	$4.5 \pm 0.9$

<sup>a</sup>These correspond to circumpolar AABW production. Carmack (1977) and Orsi et al. (1999) estimated that about 70% and 60%, respectively, of all AABW formation occurs in the Weddell Sea.

observations. Some input of AABW into the Weddell Gyre from the Indian sector is expected that could conceal the AABW export east of the Scotia Sea (see discussion below), but it is unlikely that the former matches the latter in magnitude. In the (unrealistic) limit of zero heat flux, the model yields 3.1 Sv of AABW (2.5 Sv of WSBW), close to

the lower end of the range of AABW (WSBW) production estimates in Table 3. In conclusion, our diagnosed AABW formation rate of  $9.7 \pm 3.7$  Sv is significantly higher than the values obtained by Fahrbach et al. (1994), Yaremchuk et al. (1998), the chlorofluorocarbon-based estimate of Orsi et al. (1999), and the lower end of the ranges

given by Gill (1973), Carmack (1977), Weiss et al. (1979), and Meredith et al. (2001b). On the other hand, it supports the upper end of those ranges, the mass budget analysis of Orsi et al. (1999) and the estimates of Mensch et al. (1997), Sloyan and Rintoul (2001) and Hellmer and Beckmann (2001).

The model diagnoses a comparable AABW export through the Scotia Sea route and the eastern pathways (Fig. 10). This is in variance with existing views of a dominant export along the eastern pathways, but in qualitative agreement with the numerical study of Matano et al. (2002). East of the WOCE A23 section, there is a net AABW export of  $5.0 \pm 4.3$  Sv (the large error bar results from the high sensitivity of the eastern WSDW export to the net heat flux constraint), which represents about 52% of the total in the limit of no AABW inflow from the Indian sector. Of those,  $3.9 \pm 0.8$  Sv originate from the WSBW layer and  $1.1 \pm 3.5$  Sv from the WSDW layer, although the approximate confinement of WSBW to the Weddell-Enderby Abyssal Plain (Orsi et al., 1993) implies that it must entrain upward into the WSDW to escape the gyre. However, the WSDW contribution to the AABW export east of the Scotia Sea (and therefore the export itself) is likely to be an underestimate. As shown by Meredith et al. (2000), the WSDW layer at the southern end of WOCE A23 may receive an inflow of water from the Indian sector of the Southern Ocean (indicated by the question mark in Fig. 10). This inflow has been recently quantified by Hoppema et al. (2001), who estimated that as much as  $2.7 \pm 0.9$  Sv of ventilated surface water from the Indian sector is incorporated into the WSDW layer of the southern limb of the Weddell Gyre. Their result is in good agreement with the numerical model of Schodlok et al. (2001), in which 2.5 Sv of ventilated surface water from Prydz Bay in the Indian sector enter the Weddell Sea via the westward-flowing Antarctic Coastal Current. Rintoul (1998) in turn argued that no more than 25% of the circumpolar production of AABW occurs in the Indian Ocean, although it is not clear what fraction of this is exported to the Weddell Gyre.

Of the WSDW transported over the South Scotia Ridge, the Lower class ( $\gamma^n > 28.31 \text{ kg m}^{-3}$ )

cannot escape the Scotia Sea through the Georgia Passage (Arhan et al., 1999; Naveira Garabato et al., 2002) and must therefore be entrained upward into the lighter WSDW. In the model solution (LADCP-referenced geostrophic transport), a net northward flux of  $3.6 \pm 0.1$  Sv ( $4.0 \pm 0.6$  Sv) of Lower WSDW is effected over the South Scotia Ridge, representing 77% of the total WSDW export over the ridge and 37% of the net AABW export from the Weddell Sea (in the limit of no AABW inflow from the Indian sector). The area occupied by the Lower WSDW in the Scotia Sea, approximated by that enclosed by the  $\gamma^n = 28.31 \text{ kg m}^{-3}$  contour in Special Analysis Center Hamburg bottom neutral density climatology (Gouretski and Jancke, 1998), is  $6 \times 10^5 \text{ km}^2$  (Fig. 10). This implies a basin-average upwelling rate of Lower WSDW of  $6.0 \times 10^{-6} \text{ m s}^{-1}$  or  $190 \text{ m yr}^{-1}$  ( $6.7 \times 10^{-6} \text{ m s}^{-1}$  or  $210 \text{ m yr}^{-1}$  from the observed transports), which is an order of magnitude larger than many basin-scale estimates of deep upwelling rates elsewhere in the ocean and comparable to values obtained by studies of deep turbulence over narrow topographic clefts (Orsi et al., 1999, and references therein). The importance of the Scotia Sea as a region of effective and rapid ventilation of the deep ACC was first recognised by Locarnini et al. (1993). In an ad-hoc parameterisation of the upward entrainment rate of AABW, Orsi et al. (1999) identified the southern Scotia Sea as one of the sites with most vigorous deep turbulent entrainment throughout the Southern Ocean, and computed a local upwelling rate of  $1 \times 10^{-6}$ – $2.5 \times 10^{-6} \text{ m s}^{-1}$ , of the same order of magnitude as our estimate. Near-bottom upwelling rates of this magnitude are also diagnosed by the inverse model of Sloyan and Rintoul (2000) in the Atlantic sector of the Southern Ocean.

The intensity of deep upwelling in the Scotia Sea contrasts sharply with that in the eastern Weddell Gyre. There, according to our solution, a volume of WSBW of  $3.9 \pm 0.8$  Sv upwells over a region of  $4.7 \times 10^6 \text{ km}^2$  spanning the Weddell-Enderby Abyssal Plain from the WOCE A23 section to about  $50^\circ \text{E}$  (Fig. 10). This estimate corresponds to the area bounded by the  $\gamma^n = 28.40 \text{ kg m}^{-3}$  contour east of the WOCE A23 section in the Special

Analysis Center Hamburg bottom neutral-density climatology, and leads to an upward entrainment of WSBW in the eastern Weddell Gyre at a rate of  $8.3 \times 10^{-7} \text{ m s}^{-1}$ . This is an order of magnitude smaller than in the Scotia Sea and consonant with Orsi et al.'s (1999) AABW upwelling estimate of about  $5 \times 10^{-7} \text{ m s}^{-1}$  in the Weddell Gyre interior, as well as with a range of basin-scale estimates in the literature for other open ocean regions.

## 6. Conclusions

A LADCP, hydrographic and tracer survey of the South Scotia Ridge overflow reveals a pattern of northward (southward) flow on the western (eastern) side of each of the four deep passages in the ridge. The highest velocities (approaching  $50 \text{ cm s}^{-1}$ ) are observed over the western flank of the deepest gap, the Orkney Passage. The net, full-depth, LADCP-referenced geostrophic transport over the ridge is  $22 \pm 7 \text{ Sv}$  northward, with the jets on either side of the passages transporting 5–10 Sv in alternating directions. The corresponding WSDW export is  $6.7 \pm 1.7 \text{ Sv}$ , the bulk of which is effected through the Orkney Passage. This value is a factor of 4 larger than the 1.5 Sv estimated geostrophically by Locarnini et al. (1993) for the Orkney Passage, the only other observational estimate in the literature, and agrees closely with the 6.4 Sv in the numerical model of Schodlok et al. (2002).

The full-depth and WSDW transports over the South Scotia Ridge are modified to  $7 \pm 6 \text{ Sv}$  and  $4.7 \pm 0.7 \text{ Sv}$ , respectively, by a box inverse model of the western Weddell Gyre. As well as the LADCP and hydrographic data over the ridge, the model attempts to incorporate our previous oceanographic knowledge of the region, so its diagnostics may be closer to a long-term mean. The model diagnoses that  $9.7 \pm 3.7 \text{ Sv}$  of AABW are formed ( $5.8 \pm 3.0 \text{ Sv}$  of WSDW and  $3.9 \pm 0.8 \text{ Sv}$  of WSBW) in the Weddell Sea and that comparable amounts are exported over the South Scotia Ridge ( $\sim 48\%$ ) and further east ( $\sim 52\%$ ) in the limit of no AABW inflow from the Indian sector. The WSDW fraction with  $\gamma^{\theta} > 28.31 \text{ kg m}^{-3}$  exported to the Scotia Sea upwells there at a rate of about

$6 \times 10^{-6} \text{ m s}^{-1}$ , an order of magnitude larger than many basin-scale estimates of deep upwelling in the literature. In contrast, the WSBW exported to the eastern Weddell Gyre entrains upward at a rate of approximately  $8 \times 10^{-7} \text{ m s}^{-1}$ , more typical of other open ocean regions.

The AABW over the South Scotia Ridge and that in the northern limb of the Weddell Gyre at the WOCE A23 section have markedly different ventilation histories (Gordon et al., 2001; Naveira Garabato et al., 2002; Heywood and King, 2002; Schröder et al., 2002; Schodlok et al., 2002). Whereas the latter is thought to have formed off the Filchner-Ronne Ice Shelf, the former is cooler and fresher and has been ventilated in the north-western Weddell Sea (most likely near the Larsen Ice Shelf). The comparability of their export rates thereby suggests that the AABW sources in the northwestern and southwestern Weddell Sea may have matching influences in the mid-latitude ocean, the lower production rate of the north-western sources being compensated by a better access to the ocean basins to the north.

The nature of the influence, however, may be different in each case. The South Scotia Ridge WSDW overflow is exported to a region, the Scotia Sea, where vigorous deep turbulent entrainment has been shown to occur and the ACC fronts are brought into close proximity by the choke point of Drake Passage before diverging in the central part of the sea (Orsi et al., 1995). The combination of these two factors likely contributes to the dramatic cooling and freshening observed there across the deep ACC (Naveira Garabato et al., 2002), which is unparalleled in the rest of the Southern Ocean (Locarnini et al., 1993). It is also possible that the strong deep upwelling in the Scotia Sea is intimately linked to the frontal divergence in the region. Although some WSDW escapes the Scotia Sea through the Georgia Passage and invades the southern area of the western Georgia Basin (Arhan et al., 1999), its detection at the entry to the Malvinas Chasm (Fig. 1) suggests that it may constitute the bulk of the WSDW penetrating the chasm and upwell there (Naveira Garabato et al., 2002), further modifying the deep ACC. Significantly, the above water-mass modifications take place immediately

upstream of the Argentine Basin, where the ACC system exchanges deep waters with the Subtropical Gyre.

In contrast, AABW exported east of the Scotia Sea can be incorporated more directly into the global thermohaline cell. For example, AABW from the South Sandwich Trench route spreads into the northern part of the western Georgia Basin, where the deepest passages linking the Georgia and Argentine Basins are found (Arhan et al., 1999), and accounts for the renewal of the AABW layer of the deep western boundary current in the Argentine Basin. We thus propose that, when analysing teleconnections between the Weddell Sea and the global ocean, the comparable transports, different origins and distinct upwelling rates of the AABW exported via the Scotia Sea and further east are crucial factors to consider.

### Acknowledgements

The ALBATROSS cruise and the WOCE A23 section were funded by the Natural Environment Research Council grant GR3/11654 and UK WOCE Special Topic grant GST/02/575, respectively. We are indebted to M. P. Meredith for discussions on deep turbulent mixing and to P. Klein for useful feedback on the dynamics of ridge overflows. We thankfully acknowledge A. H. Orsi for providing the digitised frontal positions of Orsi et al. (1995). The manuscript benefited from the comments of H. H. Hellmer and the careful reviews of R. A. Locarnini and two anonymous reviewers.

### References

- Arhan, M., Heywood, K.J., King, B.A., 1999. The deep waters from the Southern Ocean at the entry to the Argentine Basin. *Deep-Sea Research II* 46, 475–499.
- Barber, M., Crane, D., 1995. Current flow in the north-west Weddell Sea. *Antarctic Science* 7, 39–50.
- Beckmann, A., Hellmer, H.H., Timmermann, R., 1999. A numerical model of the Weddell Sea: large-scale circulation and water mass distribution. *Journal of Geophysical Research* 104, 23375–23391.
- Broecker, W.S., Peacock, S.L., Walker, S., Weiss, R., Fahrbach, E., Schroeder, M., Mikolajewicz, U., Heinze, C., Key, R., Peng, T.-H., Rubin, S., 1998. How much deep water is formed in the Southern Ocean? *Journal of Geophysical Research* 103, 15833–15843.
- Carmack, E.C., 1977. Water characteristics of the Southern Ocean south of the Polar Front. In: Angel, M. (Ed.), *A Voyage of Discovery, George Deacon 70th Anniversary Volume*. Pergamon Press, Oxford, pp. 15–41.
- Carmack, E.C., Foster, T.D., 1975. On the flow of water out of the Weddell Sea. *Deep-Sea Research* 22, 711–724.
- Egbert, G.D., Bennett, A.F., Foreman, M.G.G., 1994. TOPEX/POSEIDON tides estimated using a global inverse model. *Journal of Geophysical Research* 99, 24821–24852.
- Fahrbach, E., Rohardt, G., Krause, G., 1992. The Antarctic Coastal Current in the southeastern Weddell Sea. *Polar Biology* 12, 171–182.
- Fahrbach, E., Rohardt, G., Schröder, M., Strass, V., 1994. Transport and structure of the Weddell Gyre. *Annales Geophysicae* 12, 840–855.
- Fahrbach, E., Rohardt, G., Scheele, N., Schröder, M., Strass, V., Wisotzki, A., 1995. Formation and discharge of deep and bottom water in the northwestern Weddell Sea. *Journal of Marine Research* 53, 515–538.
- Fahrbach, E., Harms, S., Rohardt, G., Schröder, M., Woodgate, R.A., 2001. Flow of bottom water in the northwestern Weddell Sea. *Journal of Geophysical Research* 106, 2761–2778.
- Fischer, J., Visbeck, M., 1993. Deep velocity profiling with self-contained ADCPs. *Journal of Atmospheric and Oceanic Technology* 10, 764–773.
- Foldvik, A., Gammelsrød, T., Tørresen, T., 1985. Circulation and water masses on the southern Weddell Sea shelf. In: Jacobs, S.S. (Ed.), *Oceanology of the Antarctic Continental Shelf*. Antarctic Research Series 43, pp. 5–20.
- Foster, T.D., Carmack, E.C., 1976. Frontal zone mixing and Antarctic Bottom Water formation in the southern Weddell Sea. *Deep-Sea Research* 23, 301–317.
- Friedrichs, M.A.M., 1993. Meridional circulation in the tropical North Atlantic. Woods Hole Oceanographic Institution Technical Report, WHOI-93-06.
- Gill, A., 1973. Circulation and bottom water production in the Weddell Sea. *Deep-Sea Research* 20, 111–140.
- Gordon, A.L., 1966. Potential temperature, oxygen and circulation of bottom water in the Southern Ocean. *Deep-Sea Research* 13, 1125–1138.
- Gordon, A.L., 1998. Western Weddell Sea thermohaline stratification. In: Jacobs, S.S., Weiss, R.F. (Eds.), *Ocean, Ice, and Atmosphere: Interactions at the Antarctic Continental Margin*. Antarctic Research Series 75, pp. 215–240.
- Gordon, A.L., Huber, B.A., 1990. Southern Ocean winter mixed layer. *Journal of Geophysical Research* 95, 11655–11672.
- Gordon, A.L., Huber, B.A., Hellmer, H., Field, A., 1993. Deep and bottom water of the Weddell Sea's western rim. *Science* 262, 95–97.

- Gordon, A.L., Mensch, M., Dong, Z., Smethie Jr., W.M., de Bettencourt, J., 2000. Deep and bottom water of the Bransfield Strait eastern and central basins. *Journal of Geophysical Research* 105, 11337–11346.
- Gordon, A.L., Visbeck, M., Huber, B., 2001. Export of Weddell Sea Deep and Bottom Water. *Journal of Geophysical Research* 106, 9005–9017.
- Gouretski, V., Jancke, K., 1998. A new world ocean climatology: Objective analysis on neutral surfaces. WOCE Rep. 256/17, WOCE Hydrographic Programme Special Analysis Centre, Hamburg, Germany.
- Harms, S., Fahrback, E., Strass, V.H., 2001. Sea ice transports in the Weddell Sea. *Journal of Geophysical Research* 106, 9057–9073.
- Hellerman, S., Rosenstein, M., 1983. Normal monthly wind stress over the world ocean with error estimates. *Journal of Physical Oceanography* 13, 1093–1104.
- Hellmer, H.H., Beckmann, A., 2001. The Southern Ocean: a ventilation contributor with multiple sources. *Geophysical Research Letters* 28, 2927–2930.
- Heywood, K.J., King, B.A., 1996. WOCE Section A23 cruise Report. UEA Cruise Report series No. 1, UEA publications, Norwich, UK.
- Heywood, K.J., King, B.A., 2002. Water masses and baroclinic transports in the South Atlantic and Southern Oceans. *Journal of Marine Research*, submitted for publication.
- Heywood, K.J., Stevens, D.P., 2000. ALBATROSS cruise Report. UEA Cruise Report series No. 6, UEA publications, Norwich, UK.
- Heywood, K.J., Locarnini, R.A., Frew, R.D., Dennis, P.F., King, B.A., 1998. Transport and water masses of the Antarctic Slope Front system in the eastern Weddell Sea. In: Jacobs, S.S., Weiss, R.F. (Eds.), *Ocean, Ice, and Atmosphere: Interactions at the Antarctic Continental Margin*. Antarctic Research Series 75, pp. 203–214.
- Hoppema, M., Klatt, O., Roether, W., Fahrback, E., Bulsiewicz, K., Rodehacke, C., Rohardt, G., 2001. Prominent renewal of Weddell Sea Deep Water from a remote source. *Journal of Marine Research* 59, 257–279.
- Jackett, D.R., McDougall, T.J., 1997. A neutral density variable for the world's oceans. *Journal of Physical Oceanography* 27, 237–263.
- Locarnini, R.A., Whitworth III, T., Nowlin Jr., W.D., 1993. The importance of the Scotia Sea on the outflow of Weddell Sea Deep Water. *Journal of Marine Research* 51, 135–153.
- López, O., García, M.A., Gomis, D., Rojas, P., Sospedra, J., Sánchez-Arcilla, A., 1999. Hydrographic and hydrodynamic characteristics of the eastern basin of the Bransfield Strait (Antarctica). *Deep-Sea Research I* 46, 1755–1778.
- Lytle, V.L., Ackley, S.F., 1996. Heat flux through sea ice in the western Weddell Sea: convective and conductive transfer processes. *Journal of Geophysical Research* 101, 8853–8868.
- Martinson, D., 1994. Ocean heat and sea ice thickness in the Southern Ocean. In: Peltier, W. (Ed.), *Ice in the Climate System*. Springer, New York, pp. 597–610.
- Martinson, D.G., Iannuzzi, R.A., 1998. Antarctic ocean-ice interaction: implications from ocean bulk property distributions in the Weddell Gyre. In: Jeffries, M. (Ed.), *Antarctic Sea Ice: Physical Processes, Interactions and Variability*. Antarctic Research Series 74, pp. 243–271.
- Matano, R.P., Gordon, A.L., Muench, R.D., Palma, E.D., 2002. A numerical study of the circulation in the northwestern Weddell Sea. *Deep-Sea Research II* 49 (21), 4827–4841.
- McPhee, M.G., Kottmeier, C., Morison, J.H., 1999. Ocean heat flux in the central Weddell Sea during winter. *Journal of Physical Oceanography* 29, 1166–1179.
- Mensch, M., Bayer, R., Bullister, J.L., Schlosser, P., Weiss, R.F., 1997. The distribution of tritium and CFCs in the Weddell Sea during the mid-1980s. *Progress in Oceanography* 38, 377–414.
- Meredith, M.P., Locarnini, R.A., Van Scoy, K.A., Watson, A.J., Heywood, K.J., King, B.A., 2000. On the sources of Weddell Gyre Antarctic Bottom Water. *Journal of Geophysical Research* 105, 1093–1104.
- Meredith, M.P., Naveira Garabato, A.C., Stevens, D.P., Heywood, K.J., Sanders, R.J., 2001a. Deep and bottom waters in the eastern Scotia Sea: rapid changes in properties and circulation. *Journal of Physical Oceanography* 31, 2157–2168.
- Meredith, M.P., Watson, A.J., van Scoy, K.A., Haine, T.W.N., 2001b. Chlorofluorocarbon-derived formation rates of the deep and bottom waters of the Weddell Sea. *Journal of Geophysical Research* 106, 2899–2919.
- Morgan, P.P., 1994. Box Inverse Modelling with DOBOX 4.2. CSIRO Marine Laboratories Report 225.
- Muench, R.D., Gordon, A.L., 1995. Circulation and transport of water along the western Weddell Sea margin. *Journal of Geophysical Research* 100, 18503–18515.
- Naveira Garabato, A.C., Heywood, K.J., Stevens, D.P., 2002. Modification and pathways of Southern Ocean deep waters in the Scotia Sea. *Deep-Sea Research I* 49, 681–705.
- Orsi, A.H., Nowlin Jr., W.D., Whitworth III, T., 1993. On the circulation and stratification of the Weddell Gyre. *Deep-Sea Research I* 40, 169–203.
- Orsi, A.H., Whitworth III, T., Nowlin Jr., W.D., 1995. On the meridional extent and fronts of the Antarctic Circumpolar Current. *Deep-Sea Research I* 42, 641–673.
- Orsi, A.H., Johnson, G.C., Bullister, J.L., 1999. Circulation, mixing and production of Antarctic Bottom Water. *Progress in Oceanography* 43, 55–109.
- Pedlosky, J., 1994. Ridges and recirculations: gaps and jets. *Journal of Physical Oceanography* 24, 2703–2707.
- Petit, B., Norro, A., 2000. Seasonal evolution of sea ice and oceanic heat flux in the Weddell Sea. *Journal of Marine Systems* 27, 37–52.
- Reid, J.L., Nowlin Jr., W.D., Patzert, W.C., 1977. On the characteristics and circulation of the southwestern Atlantic Ocean. *Journal of Physical Oceanography* 7, 62–91.
- Rintoul, S.R., 1991. South Atlantic interbasin exchange. *Journal of Geophysical Research* 97, 5493–5550.
- Rintoul, S.R., 1998. On the origin and influence of Adélie Land Bottom Water. In: Jacobs, S.S., Weiss, R.F. (Eds.), *Ocean,*

- Ice, and Atmosphere. Interactions at the Antarctic Continental Margin. Antarctic Research Series 75, pp. 151–171.
- Robertson, R.A., Padman, L., Levine, M.D., 1995. Fine structure, microstructure and vertical mixing in the upper ocean in the western Weddell Sea. *Journal of Geophysical Research* 100, 18517–18536.
- Schodlok, M.P., Hellmer, H.H., Beckmann, A., 2002. On the transport, variability and origin of dense water masses crossing the South Scotia Ridge. *Deep-Sea Research II* 49 (21), 4807–4825.
- Schodlok, M.P., Rodehacke, C.B., Hellmer, H.H., Beckmann, A., 2001. On the origin of the deep CFC maximum in the eastern Weddell Sea—numerical model results. *Geophysical Research Letters* 28, 2859–2862.
- Schröder, M., Hellmer, H.H., Absy, J.M., 2002. On the near-bottom variability in the northwestern Weddell Sea. *Deep-Sea Research II* 49 (21), 4767–4790.
- Sloyan, B.M., Rintoul, S.R., 2000. Estimates of area-averaged diapycnal fluxes from basin-scale budgets. *Journal of Physical Oceanography* 30, 2320–2341.
- Sloyan, B.M., Rintoul, S.R., 2001. The Southern Ocean limb of the global deep overturning circulation. *Journal of Physical Oceanography* 31, 143–173.
- Smith, W.H.F., Sandwell, D.T., 1997. Global sea floor topography from satellite altimetry and ship depth soundings. *Science* 277, 1956–1962.
- Trenberth, K.E., Olson, J.G., Large, W.G., 1989. A global ocean wind stress climatology based on ECMWF analyses. Technical Report NCAR/TN-338+STR, National Centre for Atmospheric Research, Boulder, CO, 93pp.
- Weiss, R.F., Östlund, H.G., Craig, H., 1979. Geochemical studies of the Weddell Sea. *Deep-Sea Research* 26, 1093–1120.
- Weppernig, R., Schlosser, P., Khatiwala, S., Fairbanks, R.G., 1996. Isotope data from Ice Station Weddell: implications for deep water formation in the Weddell Sea. *Journal of Geophysical Research* 101, 25723–25740.
- Whitworth III, T., Nowlin Jr., W.D., Orsi, A.H., Locarnini, R.A., Smith, S.G., 1994. Weddell Sea Shelf Water in the Bransfield Strait and Weddell-Scotia Confluence. *Deep-Sea Research I* 41, 629–641.
- Whitworth III, T., Orsi, A.H., Kim, S.-J., Nowlin Jr., W.D., Locarnini, R.A., 1998. Water masses and mixing near the Antarctic Slope Front. In: Jacobs, S.S., Weiss, R.F. (Eds.), *Ocean, Ice, and Atmosphere: Interactions at the Antarctic Continental Margin*. Antarctic Research Series 75, pp. 1–27.
- Wunsch, C., 1996. *The Ocean Circulation Inverse Problem*. Cambridge University Press, New York.
- Yaremchuk, M., Nechaev, D., Schröter, J., Fahrback, E., 1998. A dynamically consistent analysis of circulation and transports in the southwestern Weddell Sea. *Annales Geophysicae* 16, 1024–1038.